Received: 8 July 2024 | Revised: 1 November 2024 | Accepted: 6 November 2024

DOI: 10.1002/esp.6037

RESEARCH ARTICLE

ESPL WILEY

Subglacial hydrology insights from eskers developed atop soft beds of the Laurentide ice sheet

Francisca A. Núñez Ferreira[1] | Lucas K. Zoet[1] | J. Elmo Rawling III[2] | Marianne Haseloff[1] | Matt Rehwald[2] | David J. Ullman[3]

[1]Department of Geoscience, University of Wisconsin-Madison, Madison, WI, USA

[2]Wisconsin Geological and Natural History Survey, University of Wisconsin-Madison, Madison, WI, USA

[3]Department of Geoscience, Northland College, Ashland, WI, USA

Correspondence
Francisca A. Núñez Ferreira, Department of Geoscience, University of Wisconsin-Madison, 1215 W. Dayton, Madison, WI, USA.
Email: fanunez@wisc.edu

Funding information
Neal Silva Scholarship; USGS Great Lakes Geological Mapping Coalition award, Grant/Award Number: G21AC10682; NSF EAR Award to LKZ and MH, Grant/Award Number: 2218463; US Forest Service, Grant/Award Number: 20-CS-11091300-054

Abstract

Glacial landforms provide a valuable record from which to study the history and dynamics of past ice sheets. Eskers record paleo subglacial hydrologic and sediment transport conditions because they are composed of sediment deposited by water flowing through subglacial channels. Despite decades of study, there is still debate about their formation mechanisms and little investigation of the differences between eskers formed over soft and hard beds. To address this complexity, we analysed eskers formed over soft beds along the southern margin of the Laurentide Ice Sheet (LIS) in the Lake Superior region. This included developing a new method to calculate the basal effective pressure gradient during esker formation along the subglacial channel using grain size estimates from a 20 m tall esker exposure.

The morphometry and distribution of eskers were mapped with GIS to quantify their sinuosity and lateral spacing, and to compare those to the underlying bedrock elevation and sediment thickness. Lateral spacing decreased over time as the ice margin retreated, suggesting that melt rates increased during the LIS deglaciation. Furthermore, the relation between esker distribution and sediment thickness showed that eskers formed preferentially over thinner layers of sediment, irrespective of whether erosion occurred before their formation. The sedimentology of the Cable Esker exhibits a non-monotonic pattern in channel boundary shear stress ranging from 10 to 300 Pa, alongside a basal effective pressure gradient fluctuating between −9 to −70 Pa m^{-1}. Negative basal effective pressure gradients are consistent with esker formation in channels close to the glacier terminus, which suggests lower water pressure than normally assumed. This, combined with dynamic water level fluctuations within the esker channel, supports the theory of the formation of eskers near the ice margin.

KEYWORDS
deglaciation, effective pressure gradient, esker, Laurentide ice sheet, sedimentology, soft-bedded glaciers, subglacial hydrology

1 | INTRODUCTION

Subglacial hydrology is a fundamental factor in regulating ice dynamics because it sets the effective pressure N (ice overburden pressure minus water pressure) and sliding velocity of glaciers (Hooke, 2019; Jiskoot, 2011; Tsai et al., 2021). Basal water flow is generally categorized as either an inefficient drainage system resulting in high water pressure or an efficient drainage system resulting in low water pressure (Flowers, 2015). The spatial and temporal changes in water pressure at the bases of glaciers largely control fluctuations in the basal effective pressure and glacier slip, because the ice geometry itself changes on much longer timescales (Hooke, 2019). Therefore, an

improved understanding of subglacial water flow is crucial for predicting glacier dynamics in response to external forcing in part because all physically based sliding laws for both hard (Helanow et al., 2021; Woodard et al., 2023) and soft (Hansen et al., 2024; Zoet & Iverson, 2020) beds are explicitly dependent on the basal effective pressure.

Direct observations of subglacial hydrology from modern-day glaciers pose challenges. For example, borehole measurements obtained close to one another (e.g., Andrews et al., 2014; Rada & Schoof, 2018) often show contrasting observations regarding the efficiency of the subglacial drainage system, rendering such observations difficult to interpret within hydrologic models. However, sedimentological observations from modern and Pleistocene landforms formed at the bases of glaciers have played a crucial role in interpreting regional-scale glacier dynamics when examined through the lens of glaciological mechanics (e.g., Hooyer & Iverson, 2002; McCracken et al., 2016; Zoet et al., 2019, 2021). Many glacial landforms that result from subglacial water flow are erosional (e.g., Zoet et al., 2019) and do not preserve a sedimentological record to interpret the subglacial hydrology. Eskers, however, are an exception and thus understanding their formation process provides valuable information about subglacial hydrologic and sediment transport conditions if a method could be developed to link their deposits to glaciological conditions of interest (Beaud et al., 2018; Brennand, 2000; Burke et al., 2012; Hewitt & Creyts, 2019; Shreve, 1985).

Subglacial hydrology changes from the interior to the margin of glaciers, typically shifting from a distributed (inefficient) network to a channelized (efficient) network (Flowers, 2015; Walder & Fowler, 1994). This transition alters the water flow velocity and its potential to transport sediment. Eskers form as water flows through channelized pathways at the ice-bed interface, entraining, transporting and depositing sediment as water velocity (or boundary shear stress) changes in space and time (Hooke, 2019). During steady-state conditions, the ability of flowing water to transport sediment increases with the water flow velocity within the channel due to its effect on the boundary shear stress (Anderson & Anderson, 2010; Parker, 1990; Parker et al., 1982). Net sediment deposition within these channels results in long sinuous landforms on the landscape as glaciers retreat (Hooke, 2019). Eskers are generally oriented along the ice surface slope because the hydropotential gradient within glaciers largely mirrors the ice surface, where ice pressure is assumed to be nearly equal to the basal water pressure (Shreve, 1985). Therefore, the sediment deposited in eskers serves as a record of the evolving subglacial hydrological conditions.

There are two competing scenarios regarding sedimentation leading to esker formation within channels. Some authors suggest that sedimentation occurs synchronously within the channel (Brennand, 1994; Brennand & Shaw, 1996; Hooke & Fastook, 2007; Shreve, 1985), while others propose that it occurs time-transgressively near the margin of the ice (Beaud et al., 2018; Delaney, 2001; Hewitt & Creyts, 2019; Livingstone et al., 2015; Mäkinen, 2003; Stoker et al., 2021). Near the margin of the glacier, the channelized water flow can enter a zone where the radius of the channel is oversized (from a lack of creep closure) and the discharge will not completely fill the channel, altering conditions from one of surcharged (fully filled) to one of a partially filled channel, where pressures may range from hydraulic to atmospheric pressure (Drews et al., 2017). Consequently, the sedimentology and morphology of eskers may change due to an increased accommodation space toward the ice sheet margin, leading to esker widening or fan deposition (Mäkinen, 2003), variations in local topography, including pre-existing esker deposits and geological structures (Lindström, 1993; Stoker et al., 2021), or conduit collapses (Dewald et al., 2021).

Esker shape and lateral spacing can also provide valuable information about subglacial hydrology. Straight eskers likely form under hydrostatic pressure where water flows along a nearly straight path beneath the ice (Röthlisberger, 1972; Shreve, 1972). On the other hand, Storrar et al. (2014a) noted that the shorter eskers, deposited close to the ice margin and likely under atmospheric pressure, were more sinuous due to local topographic variations altering the course of the channel. The lateral spacing of the eskers represents the lateral distance between two parallel eskers and can be used to estimate the relationship between meltwater quantity and evacuation method for subglacial waters. For example, Boulton et al. (2007, 2009) proposed a groundwater theory for soft-bedded glaciers, where the lateral spacing between eskers is based on the interaction of basal meltwater and groundwater at the ice-bed interface. The model suggests that the lateral spacing of the eskers should increase if meltwater decreases or if the thickness of the underlying sediment increases, as subglacial meltwater can percolate into the underlying sediment. More recent numerical models, such as Hewitt (2011), suggest that the lateral spacing between eskers is proportional to basal effective pressure.

To date, the assessment of esker morphology has primarily focused on eskers developed over hard beds (Brennand, 2000; Boulton et al., 2007, 2009; Storrar et al., 2014a). Although some studies suggest that eskers form less frequently atop soft beds than atop hard beds (Clark & Walder, 1994; Storrar et al., 2014a), evidence shows that eskers can form with soft bed conditions (Frydrych, 2022; Wright, 1973). Soft beds refer to unconsolidated sediments beneath glaciers, and glacier slip involves both the sliding of the glacier over its bed and the deformation of these soft beds, influencing overall glacier dynamics (Zoet & Iverson, 2020). As a result, studying the distribution and formation of eskers atop soft beds provides valuable insights into glacier slip dynamics and the associated hydrological processes.

This paper investigates past subglacial hydrology and sediment transport by analysing eskers formed atop soft beds beneath the Laurentide Ice Sheet (LIS) during Marine Isotope Stage 2 (MIS 2). Specifically we, (1) present the first mapping of esker distribution and morphometry across the Chippewa Lobe and part of the Ontonagon Lobe, comparing these features to a regional dataset of bedrock and sediment thickness; (2) analyse the sedimentology of an esker referred to here as the Cable Esker, including its grain size distribution; and (3) estimate shear stress and basal effective pressure gradients within channels using a new method. These approaches provide new quantitative data on subglacial hydrology and enhance our understanding of esker formation atop soft beds.

2 | STUDY AREA

Eskers included in this study are located in Wisconsin, USA (see Figure 1), in the footprint of the Chippewa and Ontonagon Lobes of the MIS 2 LIS (Attig et al., 1985). Additionally, one esker (hereafter referred to as the Cable Esker) formed under the Superior Lobe at the

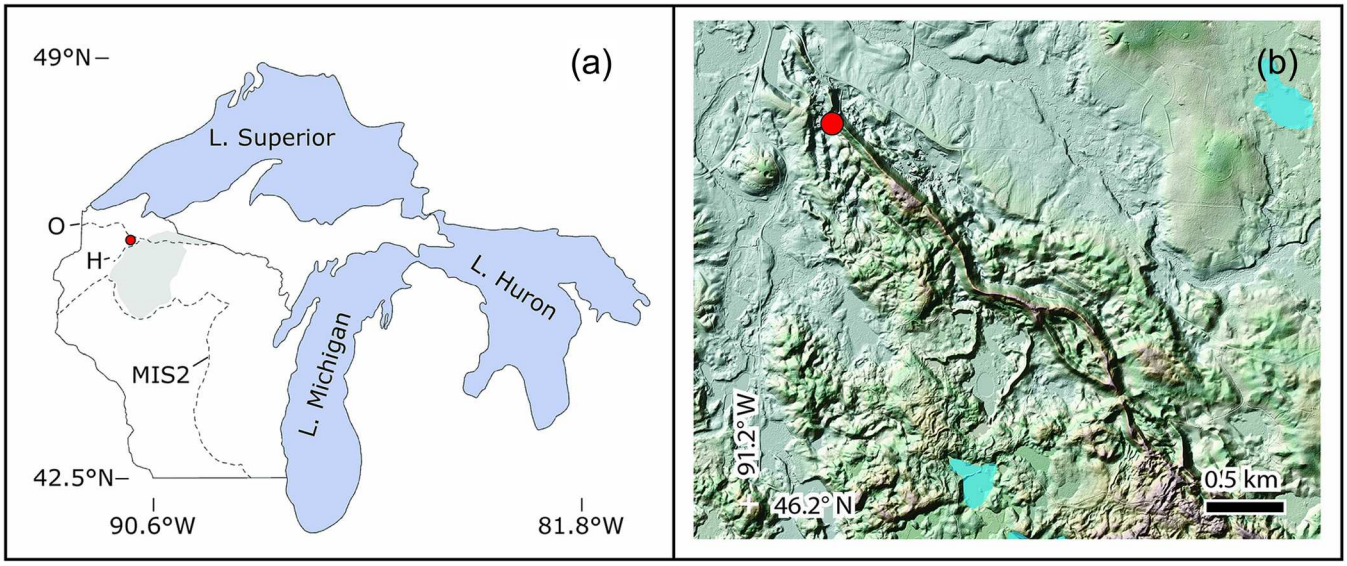

FIGURE 1 Study site. (a) Location of study area relative to the Western Great Lakes and Wisconsin. Dashed lines are MIS2, Ontonagon (O) and Hayward (H) ice margins in Wisconsin. Gray area is the study area within the footprints of the Chippewa and Ontonagon lobes in Wisconsin. Red dot is location of the Cable Esker. (b) The Cable Esker showing the location of the exposure (red dot).

Hayward ice margin (Clayton, 1984). The Cable Esker was selected for detailed examination because it was well exposed in an active aggregate mine, which allowed for the detailed study of its internal stratigraphy. Its proximity to the Chippewa Lobe (<5 km) suggests that the dynamics of this part of the Superior Lobe (e.g., bed composition, subglacial water flow, ice thickness) are likely more similar to the Chippewa Lobe than to other parts of the Superior Lobe located several hundred kilometres away.

The southern margin of the MIS 2 LIS flowed into the preexisting Lake Superior Basin in the Great Lakes region, forming terrestrial lobes that were diverted to the west (Flint, 1957; Mickelson et al., 1983; Mickelson & Colgan, 2003). As ice thickened within the Superior Basin, it overtopped a bedrock divide and flowed southward to form several sub-lobes in northern Wisconsin (Attig & Rawling, 2018). The bedrock across the study area included Precambrian crystalline rocks overlain by Paleozoic sedimentary rocks (Mudrey et al., 1982). Ice sheet models of the LIS capture large-scale dynamics, such as velocity, temperature distributions, ice thickness evolution and ice stream activity, which are influenced by the underlying geology, topography and basal hydrology (Marshall et al., 2000; Stokes et al., 2016; Stokes & Tarasov, 2010). However, they often lack the resolution needed to accurately represent the complex local behaviour of terrestrial ice streams. Therefore, this study focuses on the local geomorphology left behind by the sub-lobes in the study area.

Between approximately 25,000–11,000 years ago, the ice of the Superior and Chippewa Lobes retreated from their maximum positions, with periods of stabilization or readvance along a series of ice margins, as seen with the Wisconsin Valley and Langlade Lobes to the east (Attig & Rawling, 2018). The retreat of these lobes over a soft, deforming bed left behind distinct landforms, such as moraines, drumlins, tunnel channels and eskers, which differ in distribution from those formed by lobes sliding over hard beds (Mickelson & Colgan, 2003). Approximately 14,000 years ago, the ice retreated into the superior basin before readvancing just south of the bedrock divide to form the Ontonagon Lobe. Many of the stable ice margins were likely short-lived because any ice-marginal features associated with them are difficult to trace regionally. However, the Ontonagon Lobe readvance was likely more extensive and formed a more continuous series of ice-marginal landforms (Attig & Rawling, 2018). These three lobes deposited up to 300 m of sediment that formed the Copper Falls Formation (Syverson & Colgan, 2011). Finally, when the Superior Lobe retreated, Glacial Lake Duluth formed in the Lake Superior Basin to the north of the study area approximately ca. 10,800 cal yr BP (Breckenridge, 2013). However, there is no evidence that this glacial lake is associated with the eskers in this study.

3 | METHODOLOGY

3.1 | Remote sensing analysis

A 2 m lidar-derived elevation and hillshade models (State Cartographer's Office, 2023) were used to map eskers formed under the Chippewa and Ontonagon Lobes as polyline features in ArcGIS Pro. These were then classified based on their morphology using a modification of Banerjee & McDonald's (1975) classification system: continuous single-ridge eskers, beaded eskers and complex, multiple-crest eskers (Figure 2). For complex, multi-ridge eskers, polylines were drawn over the longest and highest ridge, while tributary eskers were mapped as separate eskers (Storrar et al., 2014a). Gaps of 0.5 to 2.5 km between continuous eskers were mapped as a new straight polyline connecting the two segments of eskers. These gaps were then grouped with esker segments to minimize distortion in the statistical analysis caused by the absence of esker ridges (Storrar et al., 2014a).

The mapped eskers were grouped into four zones based on the retreat pattern of the LIS in the study area. Eskers associated with the MIS 2 maximum and Ontonagon phases, which are continuous across the study area, were assigned to zones one and four,

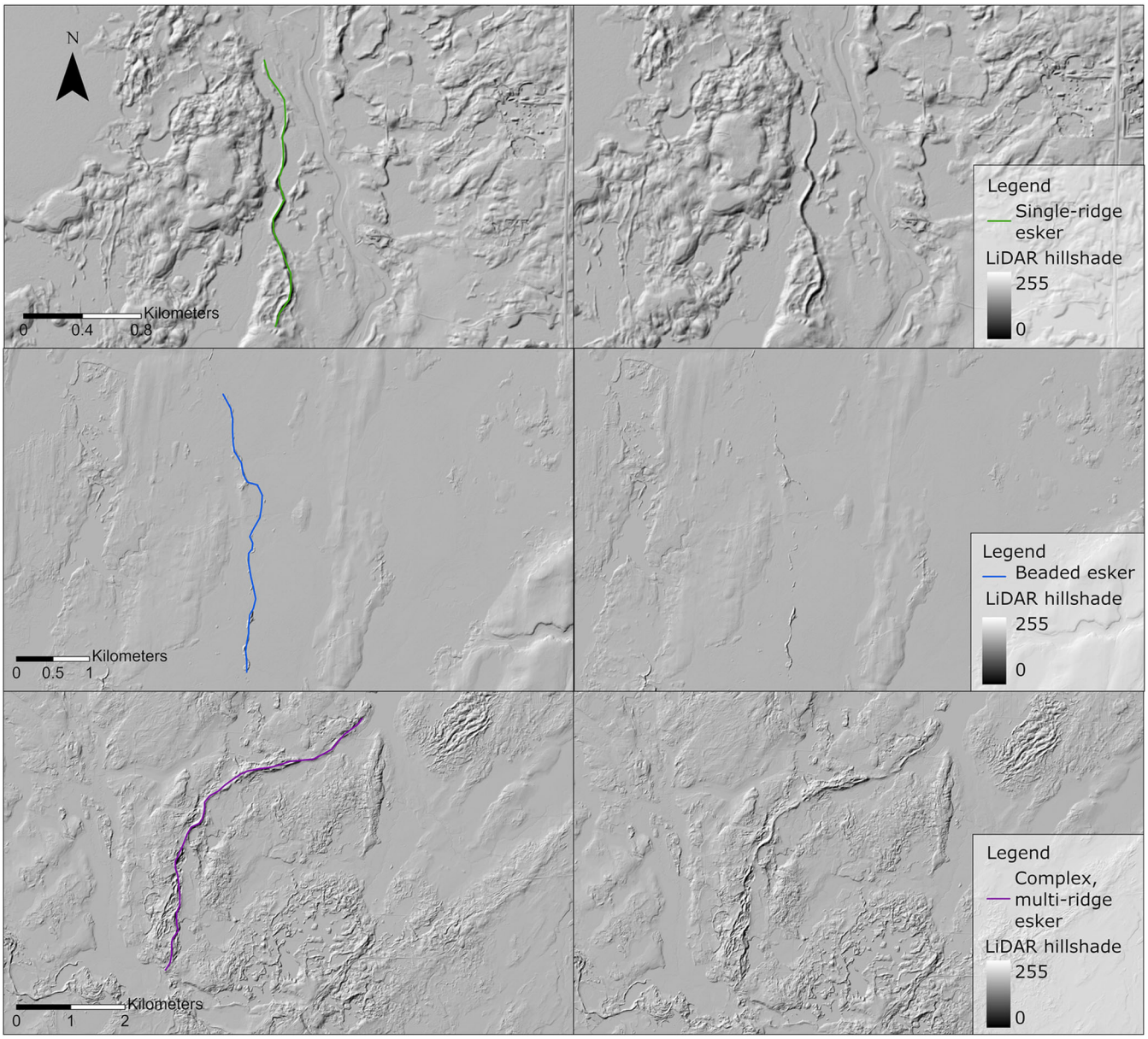

FIGURE 2 Types of eskers developed under the Chippewa lobe. Single-ridge eskers are continuous ridges, beaded eskers have gaps of <0.5 km and complex, multi-ridge eskers contain zones where the ridge bifurcates, containing more than one ridge. The left column shows the polylines over the esker while the right column shows the eskers in the hillshade. The top row is a single-ridge esker, the middle row is a beaded esker and the lowest row is a complex, multi-ridge esker.

respectively. Zones two and three follow the general orientation of the discontinuous ice-marginal landforms within those zones. All four zones are separated by an area with few or no eskers. Sinuosity, length and lateral spacing were then calculated within these zones.

The sinuosity *sn* is the dimensionless ratio of the esker length l_e to the straight-line distance l_s between its start and end points:

$$sn = \frac{l_e}{l_s} \quad (1)$$

The straight-line distance l_s was determined using the coordinates of the start and end points of each esker and calculating the Euclidian distance between them. Sinuosity was measured for both the individual esker segments as well as for grouped esker segments that shared a common path but that were segmented due to potential post-depositional erosion via proglacial water flow.

The lateral spacing between eskers was calculated for each zone (e.g. 1, 2, 3, 4) and the subsequent subzones (e.g., 1a, 1b, 1c) shown in Figure 4. Following Storrar et al. (2014a) for subzones, we selected areas of high esker density to calculate the lateral spacing, generally at two or three locations within each zone to provide a comprehensive assessment of the spatial arrangement and distribution patterns of the eskers.

Bedrock elevation and sediment thickness maps of the study area were developed from water well records (see Data S1) to compare values (e.g., bedrock elevation and sediment thickness) at the location of an esker with the average values for the entire region. This comparison was done to assess whether sediment thickness or bedrock elevation influences different types of eskers and observe variations across the area. Sediment thickness and bedrock elevation data at the esker locations were obtained using the Extract by Mask tool in ArcGIS Pro. Since the water well records used to create the

sediment thickness map were collected at points away from the eskers, the sediment thickness in the map generally represents the thickness of the sediment beneath the esker and does not include the esker itself.

Finally, the basal melt rates were calculated for each subzone throughout the study area using the lateral spacing results following Boulton et al., 2009's equation 1:

$$S = 77.8\left(\frac{T}{m}\right)^{½} \tag{2a}$$

$$T = K\,b \tag{2b}$$

where the lateral spacing between eskers, S, is related to the basal melt rate, m, and the transmissivity, T, of the substrate. The transmissivity depends on the hydraulic conductivity, K, of the basal material (Bear, 2013) and the depth of the substrate, b. For this calculation, we used the average sediment thickness beneath the specific eskers and a hydraulic conductivity of 94.67 m yr^{-1} for the sediment (Zoet et al., 2019).

3.2 | Field logging and sedimentological analysis

Mining excavations provided access to an exposure of the sediment within the Cable Esker. Even though the Cable Esker is related to the Superior Lobe, we selected it based on the good exposure and close proximity to the area related to the Chippewa Lobe (<5 km). Fourteen vertical metres of the exposure were cleared by hand tools where it could be safely accessed, and a 2 m pit was dug at the base of the exposure extending below the ground surface (Figure 3). The cleared areas were photographed, described, sampled and subdivided into units based on sedimentary textures. The sedimentary texture classification includes grain size (Wentworth, 1922), grain shape (Powers, 1953) and fabric (Boggs, 2009).

Representative samples were separated for grain-size distribution into three fractions: smaller grains (<2 mm), medium grains (2–16 mm) and larger grains (>16 mm). Samples <2 mm were analysed by laser diffraction, and samples between 2 and 16 mm were analysed using standard sieving techniques with aperture sizes of 2, 4, 6.3, 8 and 16 mm. Samples between 16 and 200 mm were measured using a ruler and scale. Grains larger than 200 mm were photographed and analysed with Image J software to obtain the length and height of the grains to estimate the area. The mass was then calculated using a density of 2.6 g cm^{-3} (Nichols, 2009), the length, height and an assumed width equal to the height of each grain. Finally, the three fractions were combined using their weight, and the d_{50} and d_{90} grain sizes were estimated from the entire range of measured grain sizes.

3.3 | Estimation of shear stress and basal effective gradient within subglacial channels

Water flowing through subglacial channels is capable of transporting and depositing sediment to form eskers. This flow is regulated by the slopes of the ice surface and bed, and variations in local effective pressure (Ng, 2000). The size fraction of sediment that can be transported is proportional to the boundary shear stress along the base of the channel. Consequently, a record of these properties and their temporal changes is preserved in the sediments that comprise the esker. Below we present a new method for estimating the status of the channelized subglacial hydraulic system from measurements of the sediments deposited within an esker.

The channel boundary shear stress τ_b is estimated through the application of the Shields criterion (Shields, 1936):

$$\tau_{*c} = \frac{\tau_b}{(\rho_s - \rho_w)gD} \tag{3a}$$

$$\tau_b = (\rho_s - \rho_w)gD\,\tau_{*c} \tag{3b}$$

where τ_{*c} is the critical nondimensional shear stress, τ_b is the basal shear stress within the channel, ρ_s is the density of the sediment, ρ_w is the density of the water, g is gravity and D is the median grain size (d_{50}) or larger grain size (d_{90}). A constant critical shear stress of $\tau_{*c} =$ 0.045 (Miller et al., 1977; Yalin & Karahan, 1979) has been found suitable for grain sizes larger than 3 mm, indicating a Reynolds number larger than 10^2 (Lamb et al., 2008). Using this criterion an estimate of τ_b can be made from the grain size distribution measurements within each unit of the Cable Esker.

The hydraulic gradient $\frac{\partial\psi}{\partial x}$ at the glacier bed depends on the background hydraulic potential gradient $\frac{\partial\Phi}{\partial x}$ due to ice and bed topography and the effective pressure gradient $\frac{\partial N_C}{\partial x}$ within the channel (Ng, 2000):

$$\frac{\partial\psi}{\partial x} = \frac{\partial\Phi}{\partial x} + \frac{\partial N_C}{\partial x} \tag{4}$$

The background hydraulic potential gradient is determined by the ice and bed slopes assuming water is in cryostatic equilibrium at the ice base (Zoet et al., 2019):

$$\frac{\partial\Phi}{\partial x} = \rho_i g \sin\alpha_s + (\rho_w - \rho_i)\sin\alpha_b \tag{5}$$

Here, ρ_i is the density of the ice, ρ_w is the density of the water, g is the gravitational constant, α_s is the ice surface slope and α_b is the bed slope.

If the basal water pressure p_w is in cryostatic equilibrium with the ice overburden pressure p_i, then the effective pressure should be zero $(N_c = p_i - p_w = 0)$ and hence $\frac{\partial N_C}{\partial x} = 0$. In this case, the hydraulic gradient is fully determined by the ice geometry gradient. However, variations away from cryostatic equilibrium generally result in non-zero effective pressure gradients $\frac{\partial N_C}{\partial x} \neq 0$.

The hydraulic gradient $\frac{\partial\psi}{\partial x}$ is also related to the basal boundary shear stress in the channel (Ng, 2000):

$$\frac{\partial\psi}{\partial x} = \frac{2\,\tau_b}{h} \tag{6}$$

where h is the channel height. Combining and rearranging equations 3–6 provides a means to estimate $\frac{\partial N_C}{\partial x}$ as follows:

FIGURE 3 The sedimentology of the esker was observed in the three marked locations of the Cable Esker. Zones (a) and (b) show the face of the esker (esker extends into and out of the page), while zone (3) shows the location of a pit excavated beneath the modern-day ground surface.

$$\frac{\partial N_C}{\partial x} = \frac{2(\rho_s - \rho_w)gD\,\tau_{*c},}{h} - (\rho_i g sin\alpha_s + (\rho_w - \rho_i) sin\alpha_b) \quad (7)$$

In places where α_s, α_b and h can be reasonably estimated and the grain size distribution can be measured, it is possible to estimate $\frac{\partial N_C}{\partial x}$. This provides critical information about bed pressurization and spatial gradients in basal effective pressure within the channel. For the region around the Cable Esker, reasonable estimates can be made for all these properties. The surface slope α_s was estimated using the reconstructions of Clark (1992), who defined the ice surface contours of the Chippewa Lobe based on geomorphic features such as moraine elevations and ice flow indicators. Clark's method is particularly effective for small-scale ice topography because it avoids common uncertainties in large ice sheet models, such as basal pressure, climate variations and subglacial hydrology. Therefore, this technique provides reliable slope estimates consistent with those proposed for the Southern lobes of the LIS. The bed slope α_b was calculated from the Lidar DEM using an average of the actual topography adjacent to the Cable Esker. The subglacial channel height can be constrained with minimum and maximum values: We estimate the minimum h using the Froude number (below) and set the maximum h equal to ½ the esker height.

An estimate of the minimum channel height, h and water velocity, u, can be made via the Froude number, F_r, if bedforms are preserved within the esker sediments via the following expression (Allen, 2009):

$$F_r = \frac{u}{\sqrt{hg}} \quad (8a)$$

$$h = \left(\frac{u}{F_r}\right)^2 g^{-1} \quad (8b)$$

In instances where bedforms such as ripples are preserved a F_r number of 0.2 is found to be stable and the d_{50} grain size fraction that comprises the ripples can be used to estimate u, for example, coarse sand typically has $u \sim = 1$ m s^{-1} (Allen, 2009).

4 | RESULTS

4.1 | Remote sensing

The eskers were categorized into four zones based on the observed distributions and known retreat paths of the Chippewa and Ontonagon Lobes (see Figure 4). Additionally, the lateral spacing was calculated in three subzones in zone 1 and two subzones in zone 2, 3 and 4.

We identified the number of different types of esker segments and the number of grouped eskers within each zone (see Table 1). For the eskers grouped along a similar path, we created one new type of classification termed multi-morphometry eskers, which are comprised of different types of the previously defined eskers. The

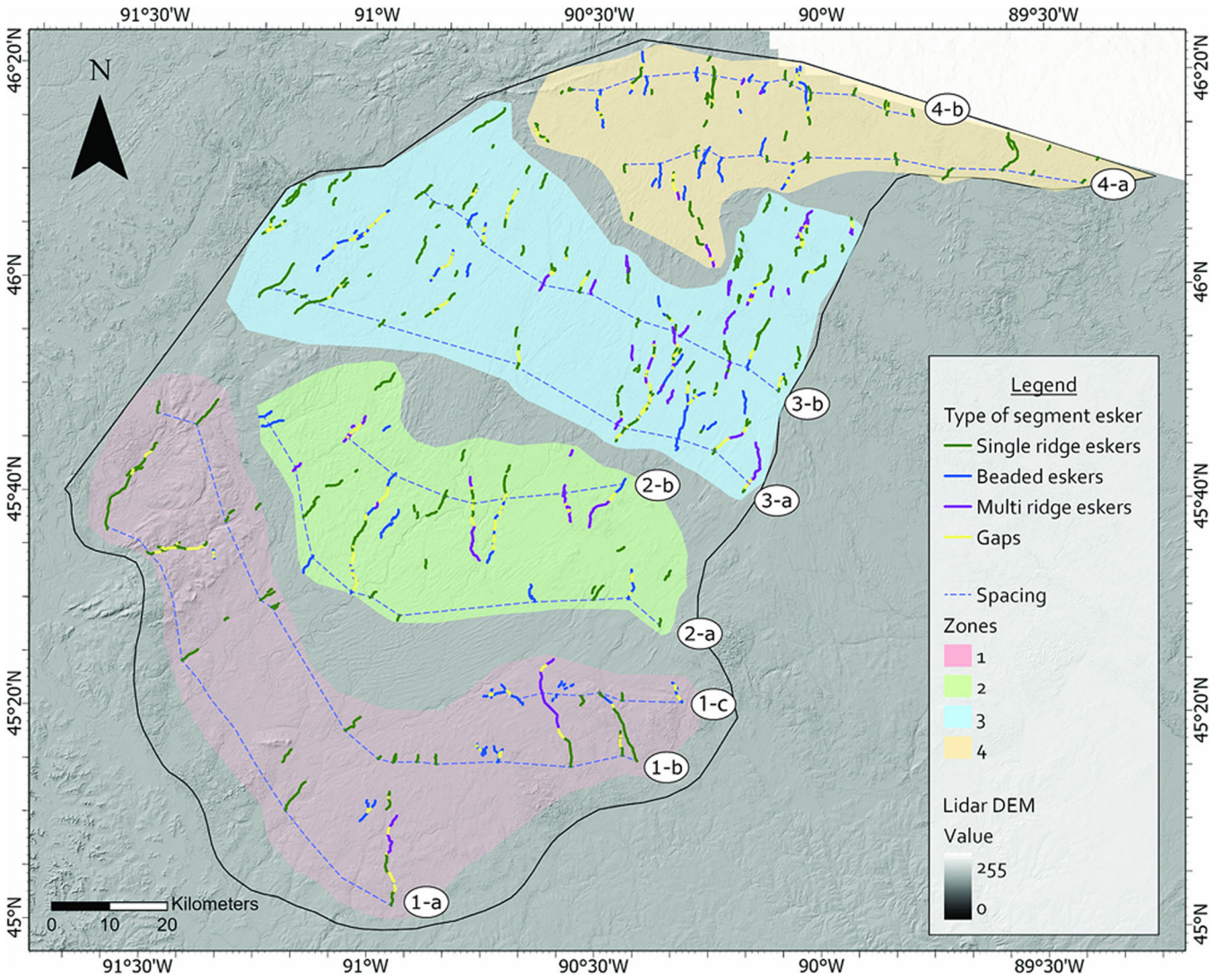

FIGURE 4 Types of eskers across the study area in each zone, with segment lines indicating lateral spacing in subzones. Labels of each subzone are shown on the map. Lidar hillshade was obtained from the State Cartographer's Office (2023).

sinuosity of segments of eskers ranged between 1 and 1.55 and the maximum decreased to 1.37 when segments of eskers along the same path were grouped (see Figure 5). However, the sinuosity remains consistent across the zones in the study area. Additionally, the sinuosity of eskers shows an inverse relationship with length, decreasing as segment length increases when eskers are grouped (see Figure 6).

Throughout the study area, bedrock elevations ranged from 268 to 535 m and eskers were mapped only in regions where the bedrock elevation ranged from 300 to 502 m (see Figure S1). The bedrock slope is less than ~2 degrees over the region, and eskers show no correspondence with the underlying bedrock's slope. Sediment thickness varies between 0 to 180 m, while beneath eskers sediment thickness ranges from 0 to 95 m (Figure 7). The average sediment thickness was calculated for the different types of eskers and for all esker segments in each zone (see Table 2).

The lateral spacing between eskers decreases from the southern to the northern zone, as well as in subzones. Conversely, melt rates increase toward the northern zone and within zones 1, 2, 3 and 4 (Figure 8).

4.2 | Sedimentology of the Cable Esker

The Cable Esker measures ~22 m maximum in height and ~120 m maximum in width. Along the exposed section, 18 sedimentary units were identified and described. Descriptions included unit thickness, sedimentological texture description, median grain size (d_{50}) and largest grain size (d_{90}) (Table 3).

Unit 1 represents the lowermost layer, while Unit 18 corresponds to the uppermost observed layer of the esker (see Figure 9). Units 1 and 2 were examined from an excavated pit below the ground level, while Unit 3 was the first unit recognized at the base of the exposure. Additionally, we made observations of units 11 through 18 at both clearings in the esker exposure.

The Cable Esker exhibited notable variations in sedimentary textures along the vertical section with grain sizes ranging from gravel (boulders) to silt (see Figure 10). The grain size distribution varied significantly, resulting in a non-monotonic pattern with median grain sizes ranging from 0.014 cm to 45 cm. With a few exceptions, grains were subrounded to rounded and had low sphericity. The units varied between well-sorted and poorly-sorted sediments, with some dis-

TABLE 1 Number of segments of eskers and grouped eskers across the study area and within each zone.

	Types of eskers	Total	Zone 1	Zone 2	Zone 3	Zone 4
Segments of eskers	Single-ridge eskers	240	36	32	121	51
	Beaded eskers	131	43	27	36	25
	Complex, multi-ridge eskers	65	6	17	32	10
Grouped eskers	Single-ridge eskers	171	23	19	85	44
	Beaded eskers	64	22	10	16	16
	Complex, multi-ridge eskers	30	0	4	20	6
	Multi-morphometry eskers	32	5	8	14	5

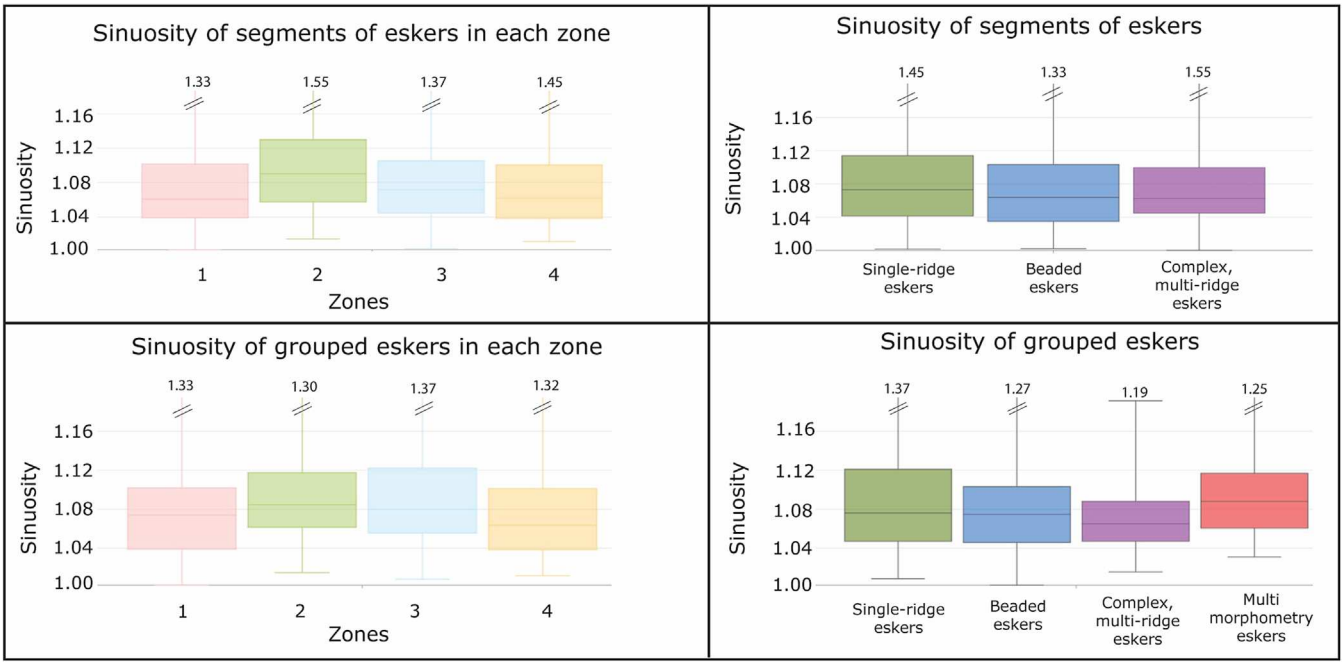

FIGURE 5 Sinuosity of segments of eskers and grouped eskers in each zone throughout the study area and sinuosity of different types of eskers.

playing distinct grain orientations. Furthermore, sedimentary structures were identified within three units of coarse sand. Unit 6 contained water escape structures from the sediment loading while Units 7 and 9 contained ripple marks.

Finally, geological contacts were observed along the esker, providing valuable insights into its stratigraphy and evolution. Sharp contacts were identified between units 7, 8, 9 and 10, and between Units 13, 14, 15 and 16. Gradual contacts were observed between Units 6 and 7, Units 11, 12 and 13 and Units 16, 17 and 18. On the large scale that spans the two different cleared sections, Unit 16 exhibits an anticlinal morphology, similar to some of the units below it. However, an exception is noted in Unit 7 where the gravel is accumulated into a channel form.

4.3 | Subglacial dynamics

The spatial effective pressure gradient and boundary shear stress within the channel can be inferred using the d_{50} or d_{90} of the Cable Esker and the parameters provided in Table 4. The thickness of the Chippewa Lobe increased by approximately 200 m in elevation over 50 km up-ice from the margin, with driving stresses ranging from 1.8 to 2.9 kPa along a 50 km flowline (Clark, 1992). The Cable Esker is approximately 4 km long and likely formed near the margin. According to Clark's (1992) Figure 8, at 10 km up ice from the margin of the Chippewa Lobe, the ice was 80 m thicker than at the margin, resulting in a surface slope of 0.008.

The basal effective pressure gradient increases linearly with grain size and shear stress (Equation 7). Using $d_{50,}$ to estimate the channel boundary shear stress it was found to range between 12 and 317 Pa within the esker's formation, reflecting variations in flow conditions both over time and space (Figure 11). Correspondingly, the basal effective pressure gradient ranges from −64 to 139 Pa m^{-1} when using the minimum channel height equal to 3 m estimated from Equation 7, and it ranges from −9 to −70 Pa m^{-1} when setting the channel height equal to half of the esker height, which is the more likely condition for most of the esker's formation (Figure 12). Additional results using d_{90} are shown in the supplemental material (Figures S2 and S3). Importantly, the basal effective pressure gradient along the channel is mostly negative and the boundary shear stress

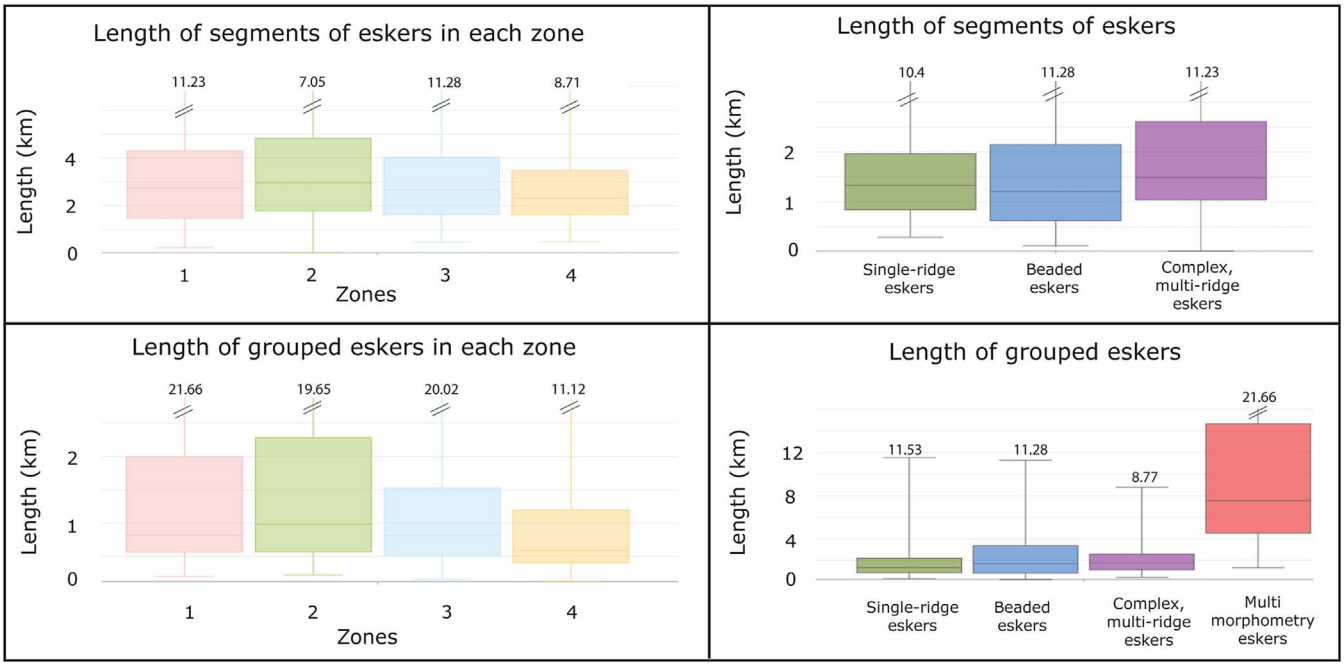

FIGURE 6 Length of segments of eskers and grouped eskers in each zone throughout the study area and length of different types of eskers.

varies non-monotonically with depth in the exposure. An exception to this trend occurs when the basal effective pressure gradient shifts to a positive value when the minimum height *h* (a 3 m high channel) is assumed when assessing the largest boulders positioned at the top of the esker. Such a small channel would not likely be able to transport these large boulders, therefore we favour the estimates of *h* equal to ½ the esker height as the more likely condition.

5 | DISCUSSION

In this study, we gain broad and detailed insights into subglacial hydrology through regional mapping and sedimentological analysis, including estimations of basal effective pressure gradient. We found that eskers atop soft beds 1) tend to form over thin sediment (Figure 7 and Table 2), 2) form during ice retreat and meltwater flux increase (Figure 8), 3) are likely to form near the margin (Figures 10 and 12), 4) form during dramatically varying water flow (Figure 11), and 5) result from a negative basal effective pressure gradient generally about −9 to −70 Pa m^{-1} (Figure 12). Together, these findings indicate that an abundant but temporally variable meltwater supply during the retreat contributed to the formation of these eskers, with the effective pressure gradient being largely negative. The estimates of the negative effective pressure gradients from the Cable Esker suggest that most of the time water pressures within the channels were not in cryostatic equilibrium. Therefore, the standard practice of assuming cryostatic equilibrium where water is largely driven via surface slope (Hooke, 2019) is likely incorrect near the margin and near large subglacial channels. In these locations, transient meltwater conditions, such as fluctuating water flow rates, variations in effective pressure and episodic water storage and release, appear to dominate the subglacial hydrologic system.

The following sections contain a detailed discussion about (1) implications of esker morphometry on a regional scale, (2) the interpretation of the sedimentology of the Cable Esker, (3) implications of negative basal effective pressure gradient during esker formation and (4) a discussion about esker formation and implications for subglacial hydrology.

5.1 | Implications of esker morphometric analysis

The fragmentation of eskers has been linked to either a cessation of sedimentation or post-depositional erosion (Banerjee & McDonald, 1975). Since the eskers in our study area form over soft beds, there should be a nearly unlimited sediment supply to form continuous eskers if hydrologic conditions are favourable (Alley et al., 1997) (Figure 7). The smaller gaps (<0.5 km) in this study were not considered as we mapped beaded eskers as one single esker, however, larger gaps (0.5–3 km) were mapped but are still smaller than gaps observed in eskers formed over hard beds (<∼10 km, Storrar et al., 2014a). Therefore, we interpret these gaps as either highly erosive conditions within the channel capable of removing all the deposited material or, more likely, proglacial fluvial erosion of segments of the esker.

The sinuosity of both mapped esker segments and grouped eskers averaged approximately 1.09, falling within the typical range of 1 to 1.32 for eskers associated with hard beds (Bolduc, 1992; Burke et al., 2012; Storrar et al., 2014a). The grouped eskers related to the Chippewa Lobe exhibit a slight increase in sinuosity while maintaining relatively similar lengths from zones 1 to 3. Storrar et al. (2014a) found that straighter eskers form under hydrostatic pressure over hard beds, suggesting in our case, that lower melt rates would be expected in areas closer to zone 3. However, we observed that melt rates increase from zone 1 to zone 3, indicating that sinuosity may slightly increase in eskers developed over soft-bedded glaciers as meltwater flux increases. Zone 4 is associated with the readvance of the Ontonagon Lobe, so shorter eskers and lower sinuosity are related

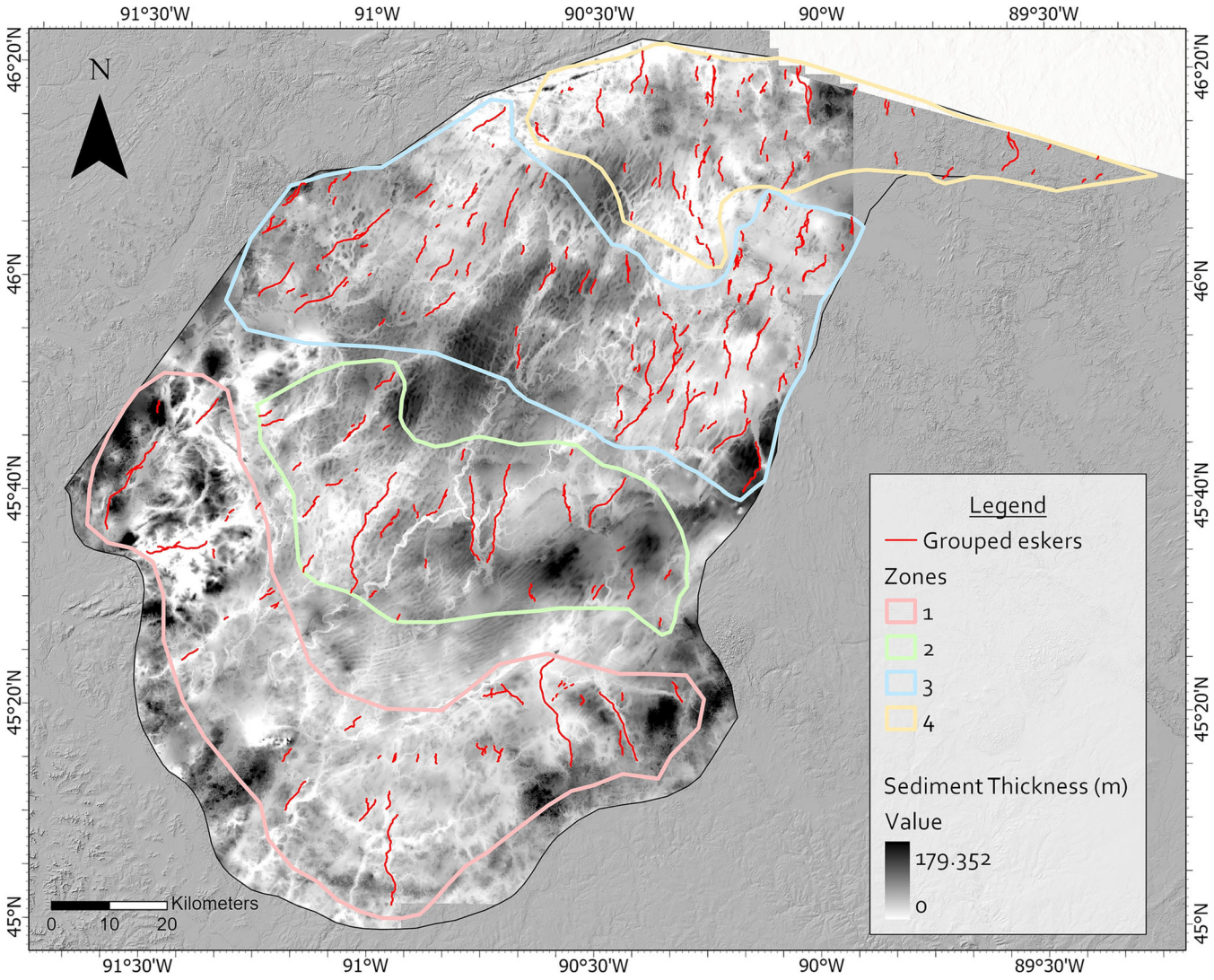

FIGURE 7 Sediment thickness across the study area. Sediment thickness was calculated by subtracting bedrock elevation from ground surface elevation. Data were derived from publicly available datasets, including the National Elevation Dataset (NED) and bedrock elevation data. Detailed information on data sources and methodology can be found in the Data S1.

TABLE 2 Average sediment thickness across the study area, under the different types of eskers and under the esker segments within each zone.

Average sediment thickness (m)	
Study area	24.6 ± 15.09
Single-ridge eskers	19 ± 12.61
Beaded eskers	15.9 ± 9.62
Complex, multi-ridge eskers	20.9 ± 12.81
Zone 1	16.4 ± 14.01
Zone 2	19.3 ± 10.99
Zone 3	20.3 ± 11.28
Zone 4	12.4 ± 9.23

to different glaciological conditions. This supports the idea that hard-bedded sliding creates efficient drainage systems with lower water pressures, while soft beds lead to less efficient water flow and pressures closer to hydrostatic equilibrium (Flowers, 2015), however still below such a bound, which may contribute to the observed variations in esker sinuosity and melt rates.

The lateral spacing of the mapped eskers shows an average of 8 km, less than eskers formed over hard beds, which typically range between 12 and 19 km (Banerjee & McDonald, 1975; Storrar et al., 2014a; Shilts et al., 1987; Bolduc, 1992). Canadian eskers formed over soft beds show no recognizable patterns (Storrar et al., 2013), but here eskers demonstrate a pattern of decreasing lateral spacing towards the North as ice retreats from the region, similar to eskers that form over hard beds in Canada (Storrar et al., 2014a, 2014b). This pattern is consistent with models (i.e., Hewitt, 2011) and observations made by Storrar et al. (2014a, 2014b), and supports the notion that as the ice retreated, meltwater increased during deglaciation, leading to closer lateral spacing towards the north (Figure 13).

Additionally, eskers exhibit a preference to develop over thin layers of till throughout the mapped area, suggesting that they form where the transmissivity of the underlying sediment was insufficient to accommodate subglacial drainage, as proposed by Boulton et al. (2009). The relationship between water supply and sediment supply is thought to play a key role in controlling esker morphometry (Burke et al., 2015; Storrar et al., 2015). However, we found that single-ridge eskers and complex multi-ridge eskers exhibit similar sediment

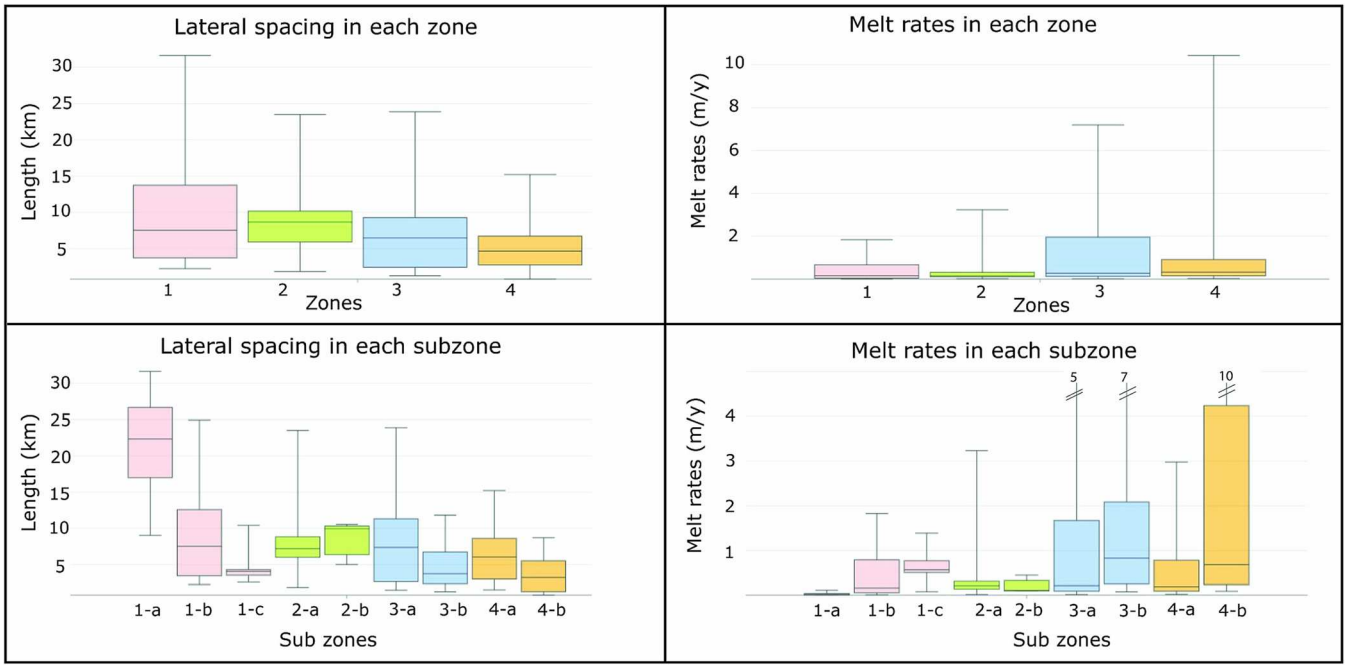

FIGURE 8 Lateral spacing length of eskers and melt rates within each zone associated with the Chippewa and Ontonagon lobes.

TABLE 3 Description of sedimentological units in the Cable Esker.

Unit	Height (cm)	Description	D_{50} (cm)	D_{90} (cm)
18	60	Boulder gravel, poorly sorted. Rounded with high sphericity. Matrix supported with some oriented grains.	45	48.5
17	100	Pebble gravel moderately sorted. Subrounded with high sphericity. Clast supported with imbricated grains.	2.3	5.6
16	50	Pebble gravel, poorly sorted. Subrounded with low sphericity. Matrix supported with random positions of grains.	6.2	9.5
15	190	Sand, very well sorted. Well-rounded with high sphericity. Clast supported with oriented grains and convoluted structure in some parts.	0.023	0.043
14	10	Massive silt, very well sorted. Well-rounded with high sphericity. Clast supported.	0.014	0.028
13	115	Cobble gravel, poorly sorted. Rounded with low sphericity. Clast supported with random positions of grains.	6.95	33
12	90	Massive pebble gravel moderately sorted. Rounded with low sphericity. Clast supported with some oriented grains.	3.98	10.2
11	65	Cobbles gravel, poorly sorted. Rounded with low sphericity. Matrix supported with random positions of grains.	9.95	15.5
10	100	Sand, very well sorted. Well-rounded with high sphericity. Clast supported with oriented grains and water scape structures.	0.033	0.061
9	10	Massive silt, very well sorted. Well-rounded with high sphericity. Clast supported.	0.006	0.014
8	40	Sand, very well sorted. Well-rounded with high sphericity. Clast supported with oriented grains and cross-bedded structures	0.061	0.094
7	15	Inverse-graded cobble gravel, moderately well sorted. Rounded with low and high sphericity. Clast supported with horizontal bedding and imbricated cobbles at the top.	7.07	10
6	20	Cobble gravel, well sorted. Rounded with high sphericity. Matrix supported with grains in random positions.	9.2	15
5	15	Pebble gravel, well sorted. Rounded with low sphericity. Clast-supported, oriented grains with tabular cross-bedded structure.	1.78	2.45
4	45	Cobble gravel, well sorted. Subangular with low sphericity grains. Matrix supported with grains in random positions.	12	13
3	100	Bottom of exposure. Pebble gravel moderately sorted. Subrounded with high sphericity. Clast supported with random positions of grains.	1.73	2.51
2	20	Top of excavated pit. Pebble gravel, well sorted. Subrounded with low sphericity grains. Clast supported with some parallel grains.	2.8	5
1	80	Excavated pit below the exposure. Transitions from pebbles at the bottom to cobbles at the top, moderately sorted. Rounded with low sphericity. Clast-supported, oriented grains with cross-bedding structure.	1.6	3.2

thicknesses, averaging 19.1 ± 12.6 m and 20.9 ± 12.8 m, respectively. This suggests that sediment thickness, and therefore sediment supply, does not significantly influence esker morphometry. Our results also show that beaded eskers are associated with slightly thinner sediment layers, averaging 16.0 ± 9.6 m, but given the standard deviations recorded, this difference is not statistically significant.

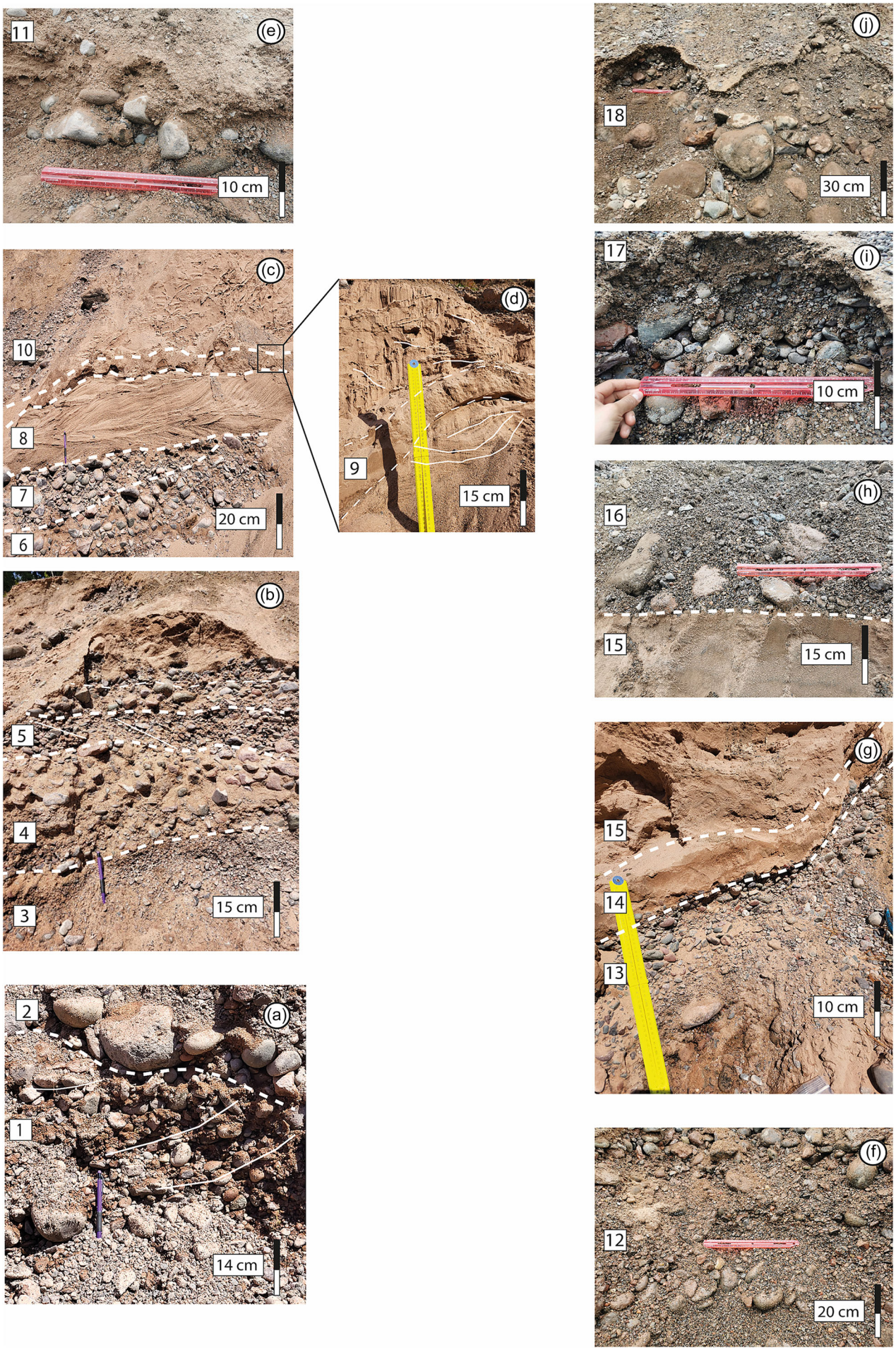

FIGURE 9 Sedimentological units along the Cable Esker.

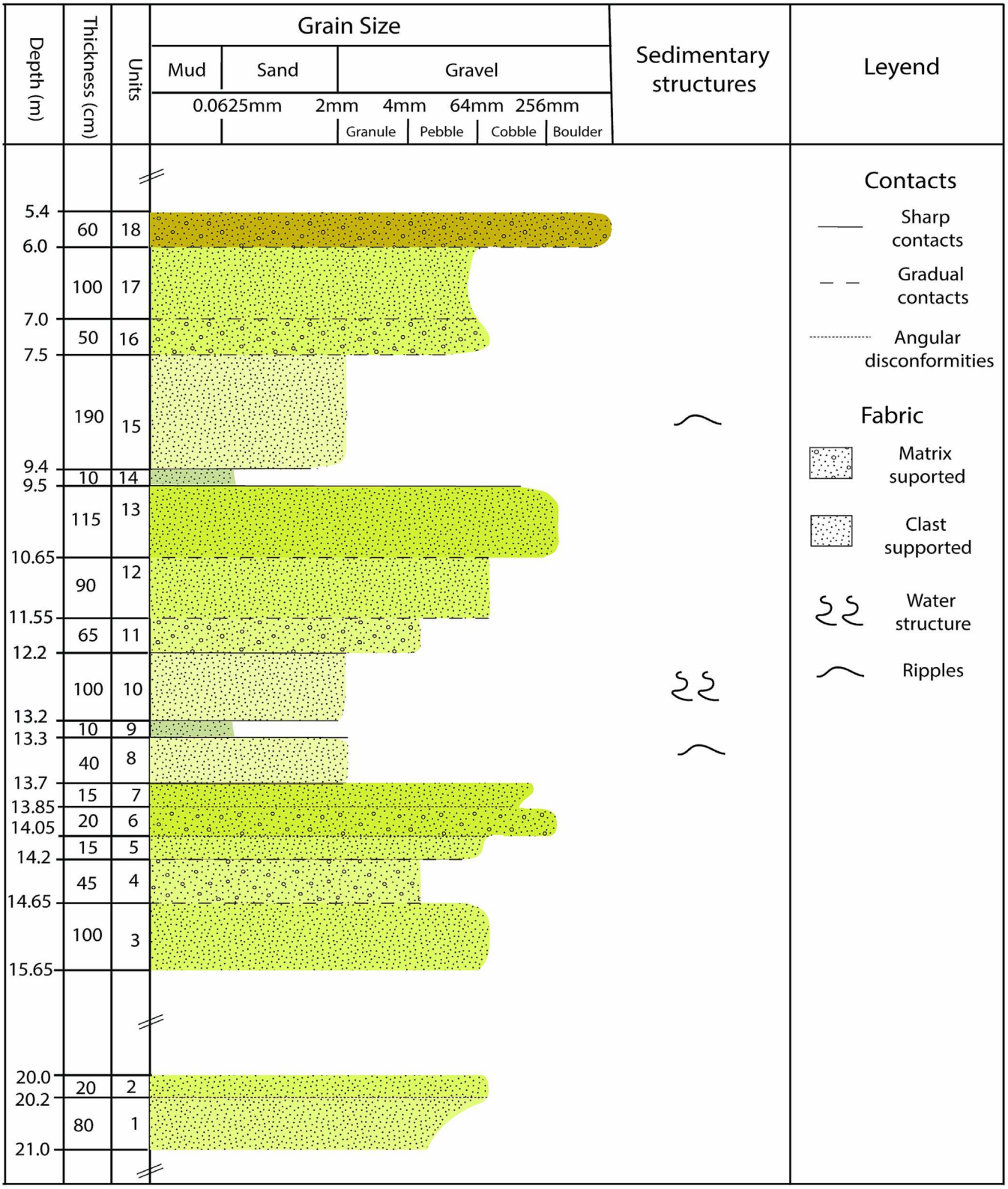

FIGURE 10 Stratigraphic column of the Cable Esker.

5.2 | Insights into the sedimentology of the Cable Esker

The nonmonotonic pattern of shear stress across the esker likely results from meltwater fluctuations influencing the basal effective pressure gradient within the channel where the esker formed. These fluctuations are reflected in the sediment texture of the esker and have been associated with depositional environments (Banerjee & McDonald, 1975; Brennand, 1994; Delaney, 2001; Warren & Ashley, 1994). Seasonal and daily temperature variations lead to changes in meltwater supply along the channel, suggesting changes in the environment of deposition between a surcharged and partially

TABLE 4 List of constants and parameters used.

Symbol	Description	Units	Value
ρ_w	Water density	kg m^{-3}	1,000
ρ_i	Ice density	kg m^{-3}	917
ρ_s	Sediment density	kg m^{-3}	2,600
τ^*_c	Critical shear stress for D larger than 3 mm	-	0.047
g	Gravity	m s^{-2}	9.8
α_s	Surface slope	-	0.008
α_b	Bed slope	-	0.0013
h	Channel height	m	3–10
$\partial\phi/\partial x$	Hydropotential gradient	kg m^{-2} s^{-2} = Pa m^{-1}	73

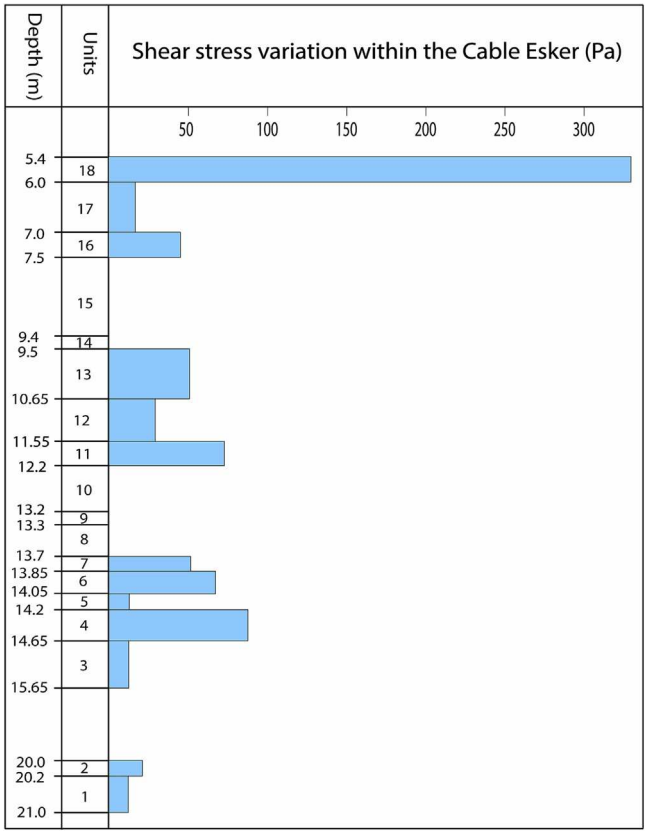

FIGURE 11 Variation in shear stress during esker formation, calculated using equation 3b with the measured d_{50} grain sizes from Table 3 and other parameters listed in Table 4.

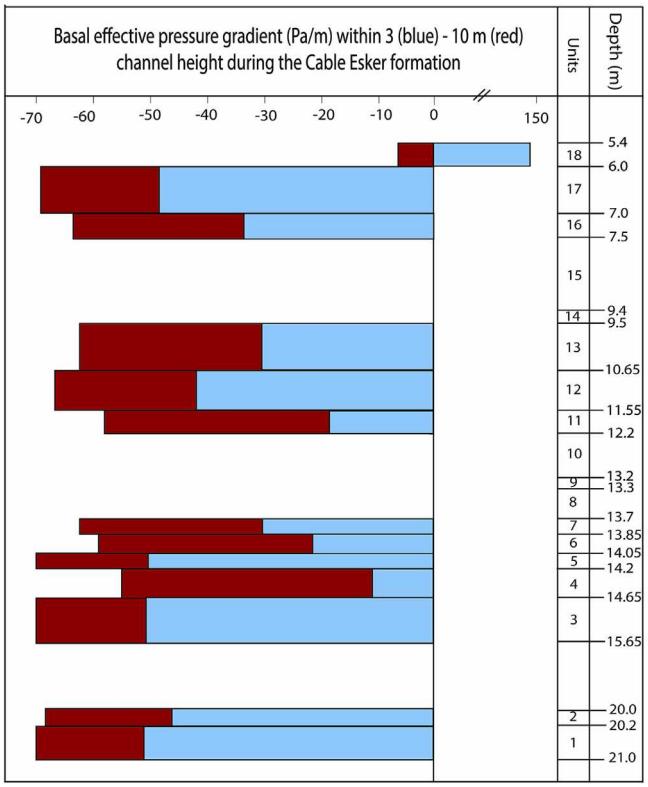

FIGURE 12 Basal effective pressure gradient along channels with heights of 3 m and 10 m during esker formation. Values are estimated using equation 7, based on the d_{50} grain sizes listed in Table 3 and the parameters shown in Table 4.

filled channel at the margin of the ice sheet (Drews et al., 2017). There are three coarsening upward sequences in the visible section of the Cable Esker: the base of the esker (units 1 to 8), the middle section, (units 9 to 13) and the upper section (units 14 to 18).

Within these sequences, we observed gravel units, which we associate with surcharge conditions, where an increased hydraulic gradient allows the transport of larger grain sizes (Mäkinen, 2003; equation 4). We relate the inversely graded gravels with imbricated clasts to re-sedimentation by turbidity currents, characterized by turbulent fluid movement, minor suspension and saltation transport (Brennand, 2000; Delaney, 2001). Given the nearly unlimited sediment supply of the Cable Esker, formed over soft beds (Alley et al., 1997), we infer that this turbidity current corresponds to increased water discharge, capable of transporting larger sediment volumes and grain sizes. Furthermore, variations in fabric among these gravels suggest fluctuating water flow dynamics. Matrix-supported units indicate a sudden increase in water flow, facilitating the simultaneous transport and deposition of various grain sizes. This results in an armouring effect, where smaller grains at depth are shielded from erosion by overlying clast-rich layers (Parker, 1990). In contrast, clast-supported units with oriented grains suggest prolonged periods of high discharge, sufficient to remove finer grains. Sand units with ripple marks at the top are associated with winter conditions (Mäkinen, 2003), marked by multiple gravity flows (Delaney, 2001), likely occurring under atmospheric pressures and reflecting a transition from surcharge to open-air, partially filled channel conditions. Silty units, on the other

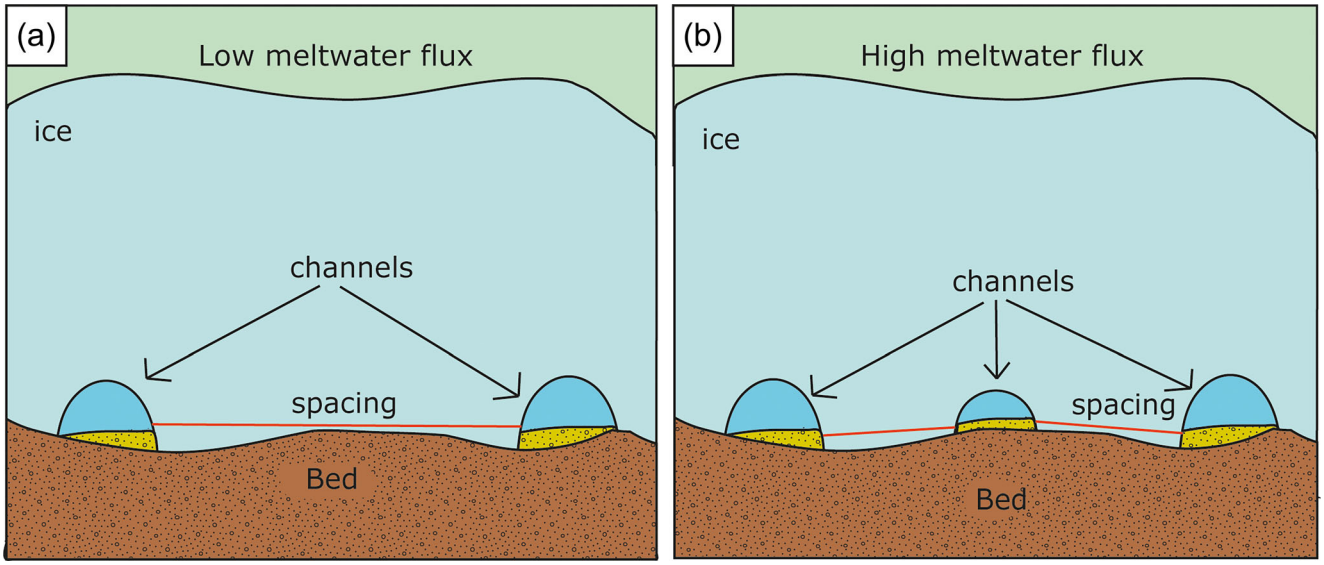

FIGURE 13 Relation between lateral spacing between eskers and meltwater flux. (a) Lower meltwater flux produces larger lateral spacing. (b) Higher meltwater flux produces smaller lateral spacing.

hand, are attributed to suspension deposition in standing water caused by underflows (Delaney, 2001). Finally, large boulders found at the top of the eskers (unit 18) may have been transported by ice and subsequently deposited through roof melting (Hewitt, 2011) or by a significantly larger turbidity current.

While it cannot be stated conclusively without dating the deposits it seems plausible that the ~20 m section examined here could have been deposited over three meltwater seasons (e.g., 3 years) with each package representing one seasonal cycle in deposition. Similar units and contacts were observed by Mäkinen (2003) who interpreted two melt seasons in an esker in SW Finland. It should be noted that there is evidence for both deposition and erosion within the channels as the sediments were reworked. Units with gradual contact between them indicate a smooth transition between water velocity and shear stress, resulting in changes in the medium grain size over time. Conversely, sharp contacts likely indicate a pause in deposition, with a decrease in discharge before the next deposition. A possible formation scenario based on the sedimentological sequence could be one in which during winter water flow is minimal and atmospheric pressure conditions led to the deposition of fine-grained materials in the Cable Esker. As temperatures warmed, increased meltwater and flow resulted in sand deposition, again with atmospheric pressure conditions as suggested by the presence of the ripple marks. In spring, the increase in melt causes a transition to surcharged conditions in which larger particles are transported and deposited. During the spring–summer season, maximum meltwater leads to full surcharge conditions and the mobilization and depositions of large clasts and boulders. These boulders armour the underlying bed, protecting it from further erosion. As the summer ends meltwater levels wane and smaller-grained sediments are again deposited atop the coarse sediment layer until winter conditions are reattained.

It is crucial to acknowledge the limitations of our study. Our observations were limited to portions of the Cable Esker that were exposed, excluding approximately 4 m between Unit 2 and Unit 3, and approximately 6 m from the top of Unit 18 to the top of the esker (see Figure 3).

5.3 | Implications of basal effective pressure gradient for esker formation

The analysis of esker grain size distribution provides a mechanism for evaluating effective pressure gradient evolution within channels using Equation 7. Within subglacial channels, sediment transport is influenced by the ice surface slope and variations in pressure within the channel. As water pressure is normally assumed to be in cryostatic equilibrium with the ice overburden pressure (Shreve, 1985), the hydropotential gradient is largely dictated by the ice surface slope and determines the maximum carrying capacity of water flow. Applying this principle with the parameters of the Cable Esker, we theoretically expected to find grain sizes of approximately 51 cm if cryostatic equilibrium was maintained. However, our field observations reveal smaller grain sizes, demonstrating that cryostatic equilibrium was primarily not maintained and required consideration of the effective stress gradient. The negative effective pressure gradient results indicate that the water level fluctuated over a range of values below cryostatic equilibrium (as shown in Figure 12), suggesting that the system was largely under non-equilibrium conditions towards the margin, as indicated by the channel water pressure remaining below the overburden pressure. This aligns with predictions made by Hewitt (2011) esker model. The cyclic nature of the deposits likely originated from the seasonal fluctuations in meltwater input as predicted by Beaud et al. (2018). Together, these findings support the concept that eskers primarily form near the margins, and this new method provides the first estimates of effective pressure gradients within a paleo-esker.

As these estimates are based on one specific esker, further work may be conducted to analyse grain size along different types of eskers and estimate the basal effective pressure gradient in other conditions. The application of this method has a central limitation in that it requires medium grain sizes to be larger than 3 mm, but in this esker where deposits primarily consisted of gravel deposits it is generally appropriate. The method also requires some estimate of the ice-surface slope, which may be another unknown variable. Here we used previous work by Clark (1992) who had approximated the ice-surface

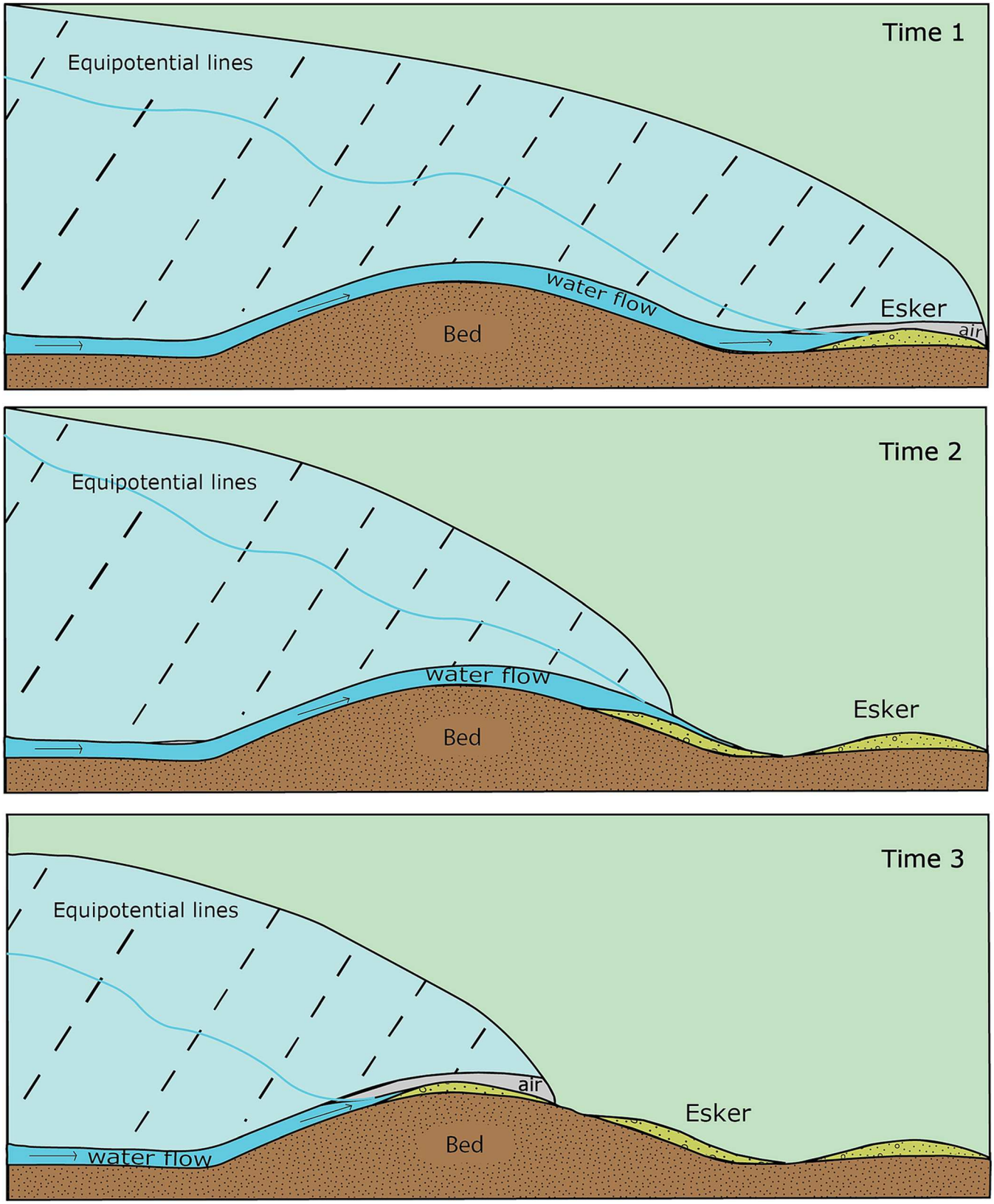

FIGURE 14 Time-transgressive model of eskers formed at the margin of the ice, including water level variations.

slope in the vicinity of the esker, but such information may not be available elsewhere in which case there would be two unknowns. For a surface slope of 0.008, our results suggest a hydropotential gradient of 73 Pa m^{-1} which falls in the normal range of 10–1,000 Pa m^{-1}, where smaller values are typically associated with ice sheets (Hewitt, 2011).

5.4 | Esker formation and subglacial hydrology implications

On the regional scale, we observed that eskers formed mainly in four zones within the mapped area with no eskers between them. Previous work has suggested that esker location is controlled by ice thickness

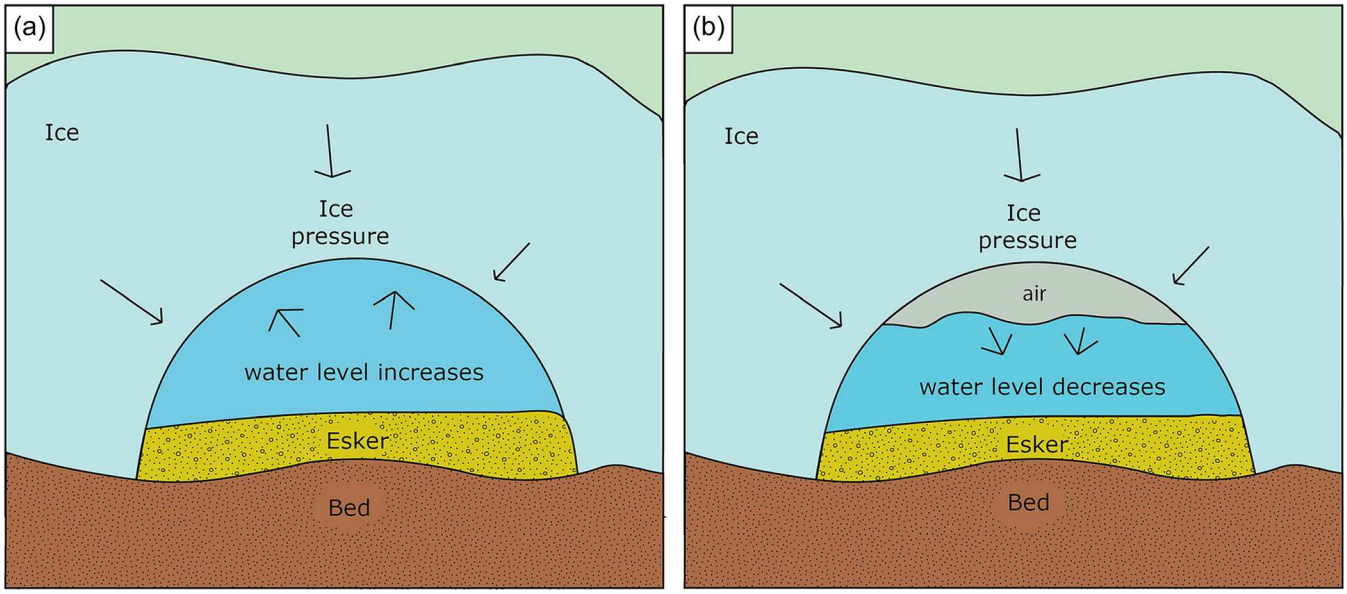

FIGURE 15 Variations in water level during esker formation (a) surcharge channel (b) partially filled channel.

(Shreve, 1972, 1985), sediment supply (Aylsworth & Shilts, 1989), water supply (Beaud et al., 2018; Burke et al., 2015; Storrar et al., 2014a, 2014b), underlying geology (Clark & Walder, 1994) and groundwater (Boulton et al., 2009), where the sediment is transported mainly through subglacial fluvial transport along channels (Delaney et al., 2019; Walder & Fowler, 1994, Overeem et al., 2017). However, there are locations with no eskers preserved, even though ice thickness, underlying geology and sediment supply were generally similar across the area (Clark, 1992). Therefore, we suggest that meltwater variability on soft beds is the dominant control of esker formation.

The sedimentology of the Cable Esker indicates transitions in depositional environments between surcharged and partially filled channels, related to a transition between R-Channels (Röthlisberger, 1972) and H-Channels (Hooke, 1984). While other studies based on morphology and sedimentology (Brennand, 2000; Frydrych, 2022) suggest that eskers can synchronously form in extensive R-channels, our results of a negative effective pressure gradient during esker formation and the small grain sizes found in the esker, indicate that these eskers likely formed only at the margin. This is because effective pressures are expected to decrease within a channel close to the ice sheet terminus, rather than further from the margin where overburden pressure is higher and water is capable of transporting larger grain sizes (for example figure 2c in Hewitt, 2011). The dynamic variations in water flow conditions affect the hydraulic gradient and the grain sizes deposited within the esker as evaluated in equation 7. The hydraulic gradient was affected by water level fluctuations, and we find evidence that the esker formed in both partially filled and surcharged channels over time. When combined these factors suggest the eskers formed time transgressively at the margin of the ice (see Figure 14) rather than synchronously over large distances.

We propose that gravel in the Cable Esker was deposited during surcharge conditions, similar to recent models suggesting that pressurized seasonal meltwater flow produces sufficient shear stress to transport boulder-size clast (Beaud et al., 2018). On the other hand, smaller grains such as sand and clay were deposited during atmospheric pressure conditions. As ripples predominantly appear during partially filled channel conditions, we expect a lower bound of 2.5 m water depth, and an upper bound of 10 m water depth, corresponding to half of the esker height, to support the higher discharge required to move large boulders along the channel. It is likely that water levels fluctuated between these two heights during esker formation (see Figure 15).

Given standard subglacial hydrologic assumptions, channelization is likely to occur near the margin (Hooke, 2019). Theoretical models suggest that channels operate at high effective pressures which decrease in proximity to the ice margin (e.g., Flowers, 2015; Hewitt, 2011). We find that at almost all times the conditions within the channel are not in cryostatic equilibrium and that temporal and spatial variations in effective pressure are dominant. These variations indicate standard steady state assumptions for water flow near the margin are likely problematic and more nuanced approaches such as Beaud et al. (2018) that incorporate meltwater variability are likely needed as they capture the dominant processes.

The channelized system increases the basal effective pressure in glaciers, and our results suggest the ice is unlikely to achieve floatation near the channels for much or all of the time, which would affect slip in the region. This finding agrees with Hewitt's (2011) model prediction about a negative spatial effective gradient but conflicts with models that assume water pressure equals the overburden stress (Shreve, 1972). Additionally, the resultant higher effective pressures near the margins have implications for glacier slip (Hansen et al., 2024; Zoet & Iverson, 2020). Zoet & Iverson (2020) have shown that the basal resistance for deformable bedded glaciers is explicitly dependent on the effective stress at the glacier base. Where high effective stress (low water pressure) inhibits slip and slows the glacier velocity. Whereas the channels in which an esker forms are quite local (only cover a small portion of the bed), they create low water pressure zones that act as a sink for water flow from the region, driving water out of the surrounding till and into the channels (see Hewitt, 2011, figures 5b & 7b, and Zoet et al., 2019 for model results of this scenario). This water flow will increase the effective stress within the pore space for some region surrounding the esker in which the till

strength will be increased, inhibiting glacier slip (Zoet et al., 2019). Such a result would contribute to a reduction in glacier flow speed at their terminus.

6 | CONCLUSIONS

The lateral spacing of eskers developed atop soft beds decreased over time as the ice retreated to the north, supporting higher melt rates and more channels available for esker formation. Moreover, the lateral spacing between eskers is smaller here than for those developed atop hard beds. As basal effective pressure gradient decreases as lateral spacing decreases, we suggest a lower N and the potential for greater slip speeds in soft beds compared to hard beds.

The sedimentology of the Cable Esker provides insights into the dynamics of subglacial fluvial sediment transport and ice sliding velocity. A non-monotonic pattern in shear stress and sedimentological textures suggests changes in water levels during deposition. The relationship between basal shear stress, grain size distribution and hydraulic gradient provides insight into how the basal effective gradient operates through channels.

The basal effective pressure gradient is negative during esker formation, indicating that eskers form at the ice margin where the channel alternates between surcharged and partially filled. Depositional conditions likely vary seasonally, with increased meltwater filling the channel and decreased meltwater resulting in a partially filled channel. Moreover, the negative basal effective pressure gradients are consistent with channelization, which suggests that water pressure within subglacial channels is lower than previously assumed, potentially leading to higher shear stress and slower sliding velocity at the margin of the ice.

ACKNOWLEDGEMENTS

We thank Natasha Morgan-Witts and Elizabeth Ives for their assistance with fieldwork, and Alan Amundson, the owner of the esker pit, for allowing us access to his land. We thank two anonymous reviewers for helpful comments that greatly improved the clarity of the manuscript. This work was partially supported by the Neal Silva Scholarship, the USGS Great Lakes Geological Mapping Coalition award number G21AC10682, the NSF EAR Award Number 2218463 to LKZ and MH, and the US Forest Service award number 20-CS-11091300-054. Data generated through this project can be obtained at the following link: https://minds.wisconsin.edu/handle/1793/89616 and DEMs can be obtained from https://www.sco.wisc.edu/data/elevationlidar/.

ORCID

Francisca A. Núñez Ferreira https://orcid.org/0009-0002-0013-0369

Lucas K. Zoet https://orcid.org/0000-0002-9635-4051

Matt Rehwald https://orcid.org/0000-0002-9380-3472

REFERENCES

Allen, P.A. (2009) *Earth surface processes*. Hoboken, NJ: John Wiley & Sons.

Alley, R.B., Cuffey, K.M., Evenson, E.B., Strasser, J.C., Lawson, D.E. & Larson, G.J. (1997) How glaciers entrain and transport basal sediment: physical constraints. *Quaternary Science Reviews*, 16(9), 1017–1038. Available from: https://doi.org/10.1016/S0277-3791(97)00034-6

Anderson, R. S., & Anderson, S. P. (2010). *Geomorphology: the mechanics and chemistry of landscapes*. Cambridge, UK: Cambridge University Press. Available from: https://doi.org/10.1017/CBO9780511794827

Andrews, L.C., Catania, G.A., Hoffman, M.J., Gulley, J.D., Lüthi, M.P., Ryser, C., et al. (2014) Direct observations of evolving subglacial drainage beneath the Greenland ice sheet. *Nature*, 514(7520), 80–83. Available from: https://doi.org/10.1038/nature13796

Attig, J.W. & Rawling, J.E. (2018) Influence of persistent buried ice on late glacial landscape development in part of Wisconsin's Northern Highlands. In: Kehew, A.E. & Curry, B.B. (Eds.) *Quaternary glaciation of the Great Lakes region: process, landforms, sediments, and chronology*, Vol. 530. Boulder, CO: Geological Society of America, pp. 103–114. Available from: https://doi.org/10.1130/2017.2530(05)

Attig, J.W., Clayton, L. & Mickelson, D.M. (1985) Correlation of late Wisconsin glacial phases in the western Great Lakes area. *Geological Society of America Bulletin*, 96(12), 1585. Available from: https://doi.org/10.1130/0016-7606(1985)96<1585:colwgp>2.0.co;2

Aylsworth, J.M. & Shilts, W. (1989) *Glacial features around the Keewatin ice divide: districts of Mackenzie and Keewatin*, Vol. 88. Ottawa, Canada: Geological Survey of Canada.

Banerjee, I. & McDonald, B.C. (1975) Nature of esker sedimentation. In: Joplin, A.V. & MacDonald, B.C. (Eds.) *Glaciofluvial and Glacilacustrine Sedimentation*. Buffalo, NY: SEPM, pp. 304–320. Available from: https://doi.org/10.2110/pec.75.23.0132

Bear, J. (2013). *Dynamics of fluids in porous media* (2nd ed.). New York, NY: American Elsevier.

Beaud, F., Flowers, G.E. & Venditti, J.G. (2018) Modeling sediment transport in ice-walled subglacial channels and its implications for esker formation and proglacial sediment yields. *Journal of Geophysical Research: Earth Surface*, 123(12), 3206–3227. Available from: https://doi.org/10.1029/2018JF004779

Boggs, S., Jr. (2009) Sedimentary textures. In: *Petrology of sedimentary rocks*. London, UK: Cambridge University Press, pp. 21–62. Available from: https://doi.org/10.1017/CBO9780511626487.003

Bolduc, A.M. (1992) *The formation of eskers based on their morphology, stratigraphy, and lithological composition*, Vol. I and II) [Doctoral dissertation. Labrador, Canada: Lehigh University.

Boulton, G.S., Hagdorn, M., Maillot, P.B. & Zatsepin, S. (2009) Drainage beneath ice sheets: groundwater–channel coupling, and the origin of esker systems from former ice sheets. *Quaternary Science Reviews*, 28(7–8), 621–638. Available from: https://doi.org/10.1016/j.quascirev.2008.05.009

Boulton, G.S., Lunn, R., Vidstrand, P. & Zatsepin, S. (2007) Subglacial drainage by groundwater-channel coupling, and the origin of esker systems: part 1—glaciological observations. *Quaternary Science Reviews*, 26(7–8), 1067–1090. Available from: https://doi.org/10.1016/j.quascirev.2007.01.007

Breckenridge, A. (2013) An analysis of the late glacial lake levels within the western Lake Superior basin based on digital elevation models. *Quaternary Research*, 80(3), 383–395. Available from: https://doi.org/10.1016/j.yqres.2013.09.001

Brennand, T.A. (1994) Macroforms, large bedforms and rhythmic sedimentary sequences in subglacial eskers, south-Central Ontario: implications for esker genesis and meltwater regime. *Sedimentary Geology*, 91(1–4), 9–55. Available from: https://doi.org/10.1016/0037-0738(94)90122-8

Brennand, T.A. (2000) Deglacial meltwater drainage and glaciodynamics: inferences from Laurentide eskers, Canada. *Geomorphology*, 32(3–4), 263–293. Available from: https://doi.org/10.1016/S0169-555X(99)00100-2

Brennand, T.A. & Shaw, J. (1996) The Harricana glaciofluvial complex, Abitibi region, Quebec: its genesis and implications for meltwater regime and ice-sheet dynamics. *Sedimentary Geology*, 102(3–4), 221–262. Available from: https://doi.org/10.1016/0037-0738(95)00069-0

Burke, M.J., Brennand, T.A. & Perkins, A.J. (2012) Transient subglacial hydrology of a thin ice sheet: insights from the chasm esker, British

Columbia, Canada. *Quaternary Science Reviews*, 58, 30–55. Available from: https://doi.org/10.1016/j.quascirev.2012.09.004

Burke, M.J., Brennand, T.A. & Sjogren, D.B. (2015) The role of sediment supply in esker formation and ice tunnel evolution. *Quaternary Science Reviews*, 115, 50–77. Available from: https://doi.org/10.1016/j.quascirev.2015.02.017

Clark, P.U. (1992) Surface form of the southern Laurentide ice sheet and its implications to ice-sheet dynamics. *Geological Society of America Bulletin*, 104(5), 595–605. Available from: https://doi.org/10.1130/0016-7606(1992)104<0595:SFOTSL>2.3.CO;2

Clark, P.U. & Walder, J.S. (1994) Subglacial drainage, eskers, and deforming beds beneath the Laurentide and Eurasian ice sheets. *Geological Society of America Bulletin*, 106(2), 304–314. Available from: https://doi.org/10.1130/0016-7606(1994)106<0304:SDEADB>2.3.CO;2

Clayton, L. (1984) Pleistocene geology of the Superior Region, Wisconsin. Wisconsin Geological and Natural History Survey Information Circular 46, 40 p., 1 pl., scale 1:250,000.

Delaney, I., Werder, M.A. & Farinotti, D. (2019) A numerical model for fluvial transport of subglacial sediment. *Journal of Geophysical Research: Earth Surface*, 124(8), 2197–2223. Available from: https://doi.org/10.1029/2019jf005004

Delaney, C. (2001) Morphology and sedimentology of the Rooskagh esker, co. Roscommon. *Irish Journal of Earth Sciences*, 19, 5–22.

Dewald, N., Lewington, E.L., Livingstone, S.J., Clark, C.D. & Storrar, R.D. (2021) Distribution, characteristics and formation of esker enlargements. *Geomorphology*, 392, 107919. Available from: https://doi.org/10.1016/j.geomorph.2021.107919

Drews, R., Pattyn, F., Hewitt, I.J., Ng, F.S.L., Berger, S., Matsuoka, K., et al. (2017) Actively evolving subglacial conduits and eskers initiate ice shelf channels at an Antarctic grounding line. *Nature Communications*, 8(1), 15228. Available from: https://doi.org/10.1038/ncomms15228

Flint, R.F. (1957) *Glacial and Pleistocene geology*. New York, NY: Wiley.

Flowers, G.E. (2015) Modelling water flow under glaciers and ice sheets. *Proceedings of the Royal Society a: Mathematical, Physical and Engineering Sciences*, 471(2176), 20140907. Available from: https://doi.org/10.1098/rspa.2014.0907

Frydrych, M. (2022) Classification of esker morphology on soft beds in the area of the Saalian and Elsterian glaciations in Poland. *Acta Geographica Lodziensia*, 112, 45–60.

Hansen, D.D., Warburton, K.L.P., Zoet, L.K., Meyer, C.R., Rempel, A.W. & Stubblefield, A.G. (2024) Presence of frozen fringe impacts soft-bedded slip relationship. *Geophysical Research Letters*, 51(12), e2023GL107681. Available from: https://doi.org/10.1029/2023GL107681

Helanow, C., Iverson, N.R., Woodard, J.B. & Zoet, L.K. (2021) A slip law for hard-bedded glaciers derived from observed bed topography. *Science Advances*, 7(20), eabe7798. Available from: https://doi.org/10.1126/sciadv.abe7798

Hewitt, I.J. (2011) Modelling distributed and channelized subglacial drainage: the spacing of channels. *Journal of Glaciology*, 57(202), 302–314. Available from: https://doi.org/10.3189/002214311796405951

Hewitt, I.J. & Creyts, T.T. (2019) A model for the formation of eskers. *Geophysical Research Letters*, 46(12), 6673–6680. Available from: https://doi.org/10.1029/2019GL082304

Hooke, R. L. (2019). *Principles of glacier mechanics*. Cambridge, UK: Cambridge University Press. Available from: https://doi.org/10.1017/9781108698207

Hooke, R.L. & Fastook, J. (2007) Thermal conditions at the bed of the Laurentide ice sheet in Maine during deglaciation: implications for esker formation. *Journal of Glaciology*, 53(183), 646–658.

Hooke, R.L. (1984) On the role of mechanical energy in maintaining subglacial water conduits at atmospheric pressure. *Journal of Glaciology*, 30(105), 180–187. Available from: https://doi.org/10.3189/002214307784409243

Hooyer, T.S. & Iverson, N.R. (2002) Flow mechanism of the Des Moines lobe of the Laurentide ice sheet. *Journal of Glaciology*, 48(163), 575–586.

Jiskoot, H. (2011) Dynamics of glaciers. *Physical Research*, 92(B9), 9–083. Available from: https://doi.org/10.1007/978-90-481-2642-2_127

Lamb, M.P., Dietrich, W.E. & Venditti, J.G. (2008) Is the critical Shields stress for incipient sediment motion dependent on channel-bed slope? *Journal of Geophysical Research: Earth Surface*, 113(F2), 1–20. Available from: https://doi.org/10.1029/2007JF000831

Lindström, E. (1993) Esker enlargements in northern Sweden. *Geografiska Annaler: Series a, Physical Geography*, 75(3), 95–110. Available from: https://doi.org/10.1080/04353676.1993.11880388

Livingstone, S.J., Storrar, R.D., Hillier, J.K., Stokes, C.R., Clark, C.D. & Tarasov, L. (2015) An ice-sheet scale comparison of eskers with modelled subglacial drainage routes. *Geomorphology*, 246, 104–112. Available from: https://doi.org/10.1016/j.geomorph.2015.06.016

Mäkinen, J. (2003) Time-transgressive deposits of repeated depositional sequences within interlobate glaciofluvial (esker) sediments in Köyliö, SW Finland. *Sedimentology*, 50(2), 327–360. Available from: https://doi.org/10.1046/j.1365-3091.2003.00557.x

Marshall, S.J., Tarasov, L., Clarke, G.K. & Peltier, W.R. (2000) Glaciological reconstruction of the Laurentide ice sheet: physical processes and modelling challenges. *Canadian Journal of Earth Sciences*, 37(5), 769–793. Available from: https://doi.org/10.1139/e99-113

McCracken, R.G., Iverson, N.R., Benediktsson, Í.Ö., Schomacker, A., Zoet, L.K., Johnson, M.D., et al. (2016) Origin of the active drumlin field at Múlajökull, Iceland: new insights from till shear and consolidation patterns. *Quaternary Science Reviews*, 148, 243–260. Available from: https://doi.org/10.1016/j.quascirev.2016.07.008

Mickelson, D.M., Clayton, L., Fullerton, D.S. & Borns, H.W., Jr. (1983) The late Wisconsin glacial record of the Laurentide Ice Sheet in the United States. In: Porter, S.C. (Ed.) *The Late Pleistocene, United States*. Minniapolis, MN: University of Minnesota Press, pp. 3–37.

Mickelson, D.M. & Colgan, P.M. (2003) The southern Laurentide ice sheet. Development. *Quaternary Science Reviews*, 1, 1–16. Available from: https://doi.org/10.1016/S1571-0866(03)01001-7

Miller, M.C., McCave, I.N. & Komar, P. (1977) Threshold of sediment motion under unidirectional currents. *Sedimentology*, 24(4), 507–527. Available from: https://doi.org/10.1111/j.1365-3091.1977.tb00136.x

Mudrey, M.G., Brown, B.A. & Greenberg, J.K. (1982) Bedrock geology map of Wisconsin. Wisconsin Geological and Natural History Survey Regional Map M078, scale 1:1,000,000. Madison, WI.

Ng, F.S. (2000) Canals under sediment-based ice sheets. *Annals of Glaciology*, 30, 146–152. Available from: https://doi.org/10.3189/172756400781820633

Nichols, G. (2009) *Sedimentology and stratigraphy*. New York, NY: John Wiley & Sons.

Overeem, I., Hudson, B.D., Syvitski, J.P., Mikkelsen, A.B., Hasholt, B., Van Den Broeke, M.R., et al. (2017) Substantial export of suspended sediment to the global oceans from glacial erosion in Greenland. *Nature Geoscience*, 10(11), 859–863. Available from: https://doi.org/10.1038/ngeo3046

Parker, G. (1990) Surface-based bedload transport relation for gravel rivers. *Journal of Hydraulic Research*, 28(4), 417–436. Available from: https://doi.org/10.1080/00221689009499058

Parker, G., Klingeman, P.C. & McLean, D.G. (1982) Bedload and size distribution in paved gravel-bed streams. *Journal of the Hydraulics Division*, 108(4), 544–571. Available from: https://doi.org/10.1061/JYCEAJ.0005854

Powers, M.C. (1953) A new roundness scale for sedimentary particles. *Journal of Sedimentary Research*, 23(2), 117–119.

Rada, C. & Schoof, C. (2018) Channelized, distributed, and disconnected: subglacial drainage under a valley glacier in the Yukon. *The Cryosphere*, 12(8), 2609–2636. Available from: https://doi.org/10.5194/tc-12-2609-2018

Röthlisberger, H. (1972) Water pressure in intra-and subglacial channels. *Journal of Glaciology*, 11(62), 177–203. Available from: https://doi.org/10.3189/S0022143000022188

Shields, A. (1936) *Application of similarity principles and turbulence research to bed-load movement*. Berlin, Germany: Soil Conservation Service.

Shilts, W.W., Aylsworth, J.M., Kaszycki, C.A., Klassen, R.A. & Graf, W. L. (1987) Canadian shield. *Geomorphic Systems of North America*, 2, 119–161.

Shreve, R.L. (1972) Movement of water in glaciers. *Journal of Glaciology*, 11(62), 205–214. Available from: https://doi.org/10.3189/S002214300002219X

Shreve, R.L. (1985) Esker characteristics in terms of glacier physics, Katahdin esker system, Maine. *Geological Society of America Bulletin*, 96(5), 639–646. Available from: https://doi.org/10.1130/0016-7606(1985)96<639:ECITOG>2.0.CO;2

State Cartographer's Office. (2023). Wisconsin Elevation/LiDAR data. Accessed December 1, 2020, at https://www.sco.wisc.edu/data/elevationlidar/

Stoker, B.J., Livingstone, S.J., Barr, I.D., Ruffell, A., Storrar, R.D. & Roberson, S. (2021) Variations in esker morphology and internal architecture record time-transgressive deposition during ice margin retreat in Northern Ireland. *Proceedings of the Geologists' Association*, 132(4), 409–425. Available from: https://doi.org/10.1016/j.pgeola.2021.03.002

Stokes, C.R., Margold, M., Clark, C.D. & Tarasov, L. (2016) Ice stream activity scaled to ice sheet volume during Laurentide ice sheet deglaciation. *Nature*, 530(7590), 322–326. Available from: https://doi.org/10.1038/nature16947

Stokes, C.R. & Tarasov, L. (2010) Ice streaming in the Laurentide ice sheet: a first comparison between data-calibrated numerical model output and geological evidence. *Geophysical Research Letters*, 37(1), 1–5. Available from: https://doi.org/10.1029/2009GL040990

Storrar, R.D., Evans, D.J., Stokes, C.R. & Ewertowski, M. (2015) Controls on the location, morphology and evolution of complex esker systems at decadal timescales, Breiðamerkurjökull, Southeast Iceland. *Earth Surface Processes and Landforms*, 40(11), 1421–1438. Available from: https://doi.org/10.1002/esp.3725

Storrar, R.D., Stokes, C.R. & Evans, D.J. (2013) A map of Canadian eskers from Landsat satellite imagery. *Journal of Maps*, 9(3), 456–473. Available from: https://doi.org/10.1080/17445647.2013.815591

Storrar, R.D., Stokes, C.R. & Evans, D.J. (2014a) Morphometry and pattern of a large sample (> 20,000) of Canadian eskers and implications for subglacial drainage beneath ice sheets. *Quaternary Science Reviews*, 105, 1–25. Available from: https://doi.org/10.1016/j.quascirev.2014.09.013

Storrar, R.D., Stokes, C.R. & Evans, D.J. (2014b) Increased channelization of subglacial drainage during deglaciation of the Laurentide ice sheet. *Geology*, 42(3), 239–242. Available from: https://doi.org/10.1130/G35092.1

Syverson, K.M. & Colgan, P.M. (2011) The quaternary of Wisconsin: an updated review of stratigraphy, glacial history and landforms. *Developments in Quaternary Sciences*, 15, 537–552. Available from: https://doi.org/10.1016/B978-0-444-53447-7.00042-8

Tsai, V.C., Smith, L.C., Gardner, A.S. & Seroussi, H. (2021) A unified model for transient subglacial water pressure and basal sliding. *Journal of Glaciology*, 68(268), 390–400. Available from: https://doi.org/10.1017/jog.2021.103

Walder, J.S. & Fowler, A. (1994) Channelized subglacial drainage over a deformable bed. *Journal of Glaciology*, 40(134), 3–15. Available from: https://doi.org/10.3189/S0022143000003750

Warren, W.P. & Ashley, G.M. (1994) Origins of the ice-contact stratified ridges (eskers) of Ireland. *Journal of Sedimentary Research*, 64(3a), 433–449.

Wentworth, C.K. (1922) A scale of grade and class terms for clastic sediments. *The Journal of Geology*, 30(5), 377–392. Available from: https://doi.org/10.1086/622910

Woodard, J.B., Zoet, L.K., Iverson, N.R. & Helanow, C. (2023) Inferring forms of glacier slip laws from estimates of ice-bed separation during glacier slip. *Journal of Glaciology*, 69(274), 324–332. Available from: https://doi.org/10.1017/jog.2022.63

Wright, H.E. (1973) Tunnel valleys, glacial surges, and subglacial hydrology of the superior lobe, Minnesota. *Geological Society of America Memoirs*, 136, 251–276. Available from: https://doi.org/10.1130/MEM136-p251

Yalin, M.S. & Karahan, E. (1979) Inception of sediment transport. *Journal of the Hydraulics Division*, 105(11), 1433–1443. Available from: https://doi.org/10.1061/JYCEAJ.0005306

Zoet, L.K. & Iverson, N.R. (2020) A slip law for glaciers on deformable beds. *Science*, 368(6486), 76–78. Available from: https://doi.org/10.1126/science.aaz1183

Zoet, L.K., Muto, A., Rawling, J.E., III & Attig, J.W. (2019) The effects of tunnel channel formation on the Green Bay lobe, Wisconsin, USA. *Geomorphology*, 324, 36–47. Available from: https://doi.org/10.1016/j.geomorph.2018.09.021

Zoet, L.K., Rawling, J.E., III, Woodard, J.B., Barrette, N. & Mickelson, D.M. (2021) Factors that contribute to the elongation of drumlins beneath the Green Bay lobe, Laurentide ice sheet. *Earth Surface Processes and Landforms*, 46(13), 2540–2550. Available from: https://doi.org/10.1002/esp.5192

SUPPORTING INFORMATION

Additional supporting information can be found online in the Supporting Information section at the end of this article.

How to cite this article: Núñez Ferreira, F.A., Zoet, L.K., Rawling, J.E. III, Haseloff, M., Rehwald, M. & Ullman, D.J. (2025) Subglacial hydrology insights from eskers developed atop soft beds of the Laurentide ice sheet. *Earth Surface Processes and Landforms*, 50(1), e6037. Available from: https://doi.org/10.1002/esp.6037